A Novel Staged Warm Gas Thruster for CubeSats: Final Report

Group 9: Spencer Powers, Connor Powers, Michael Mastrangelo, Kamyar Zarkoub, Spencer Wing

AME 441AL: Senior Projects Laboratory

November 19, 2020

Department of Aerospace and Mechanical Engineering
Viterbi School of Engineering, University of Southern California

Abstract

Cold gas thrusters are a popular propulsion method for CubeSats due to their simplicity and reliability, but their performance is poor compared to combustive and electric propulsion alternatives. Warm gas thrusters add a heating element to this architecture to improve the thruster efficiency, but existing heating techniques are either inefficient or needlessly complex. A new warm gas thruster design is introduced that builds upon the VACCO MiPS, an industry standard cold gas propulsion module, while outperforming CHIPS, an industry-standard resistojet warm gas thruster. An ideal in-space design was produced by integrating progressively more complex thermal analysis tools with thruster performance calculations to produce an optimized 1U configuration capable of delivering 478 N-sec of impulse in periodic 40 mN-sec blowdowns. This represents a 90% gain in delivered impulse over the MiPS, enabling the same complex formation-flying missions as CHIPS with 80% less heater power. The staged, cyclic nature of the proposed system is designed to meet temporal inter-maneuver requirements of FIONA, a modern formation flying algorithm used in the CanX-4 and CanX-5 Cubesat missions. A brassboard system was then designed to test key thruster behavior in a thermally analogous laboratory environment.

Contents

List of Figures

List of Tables

Symbols

$\bar{I_{sp}}$	Average Specific Impulse
I_{tot}	Total Impulse
I_{blow}	Blowdown Impulse
$\bar{F_T}$	Average Thrust
V_{int}	Intermediate Tank Volume
t_{ins}	Intermediate Tank Insulation Thickness
c_p	Specific Heat Capacity
$T_{prop,max}$	Maximum Heated Propellant Temperature
$T_{ins,max}$	Maximum Insulation Operating Temperature
T_{bulk}	Propellant Bulk Storage Temperature
ρ	Propellant Density
u	Propellant Velocity
D_t	Nozzle Throat Diameter
μ	Propellant Dynamic Viscosity
P	Propellant Pressure
γ	Propellant Ratio of Specific Heats
g_E	Gravitational Acceleration
L_{con}	Connector Length

1 Introduction

Effects of the COVID-19 pandemic notwithstanding, the commercial space industry is experiencing a period of massive growth, buoyed by a recent surge in commercial space companies competing ferociously in areas from spacecraft propulsion to satellite design and operation. While some focus on large-scale spacecraft for missions to the moon and Mars, many are turning their attention to Earth-orbiting applications, and within this sphere the CubeSat has begun to dominate the satellite population. Comprised of standardized, modular 10x10x10 cm volumes, CubeSat-based satellite systems offer cheaper replacement and greater failure resistance than massive and costly single-satellite designs; if one of a fleet of CubeSats fails, portions of mission capabilities could be preserved, and a replacement can be produced and launched rapidly and economically. In traditional single-satellite systems, failure of the satellite means complete loss of the mission, and there is a higher cost in replacing the entire satellite. Due to these advantages, the CubeSat satellite market is expected to increase from $152 million in 2018 to $375 million in 2023 [1].

Spacecraft propulsion is a diverse field ranging from chemical propulsion for launch vehicles to electric propulsion for deep space exploration. Due to the tight volume and power constraints imposed by standardized CubeSat design requirements, these satellites often use one of the simplest propulsion systems in this wide array: cold gas thrusters. Cold gas thrusters work by expelling pressurized gas through a nozzle via a simple blowdown system. While being highly reliable, the nature of their blowdown-based approach yields decaying propellant pressures and temperatures at the nozzle input, subsequently yielding a decay in overall thruster performance over the course of burns and lower overall efficiencies than their combustive counterparts. An industry-standard example of a cold gas thruster for CubeSats is the VACCO Standard Micro Propulsion System (MiPS), which utilizes the self-pressurizing refrigerant R134a as its propellant [2].

In an attempt to mitigate the performance-damaging side effects of cold gas systems, the concept of the warm gas thruster has begun to find maturity in development and application. These propulsion systems are nearly identical to cold gas thrusters, except they use electrical power to heat the propellant, which positively affects the efficiency of the thruster. Naturally, this increased efficiency comes at a cost of increased power requirements. A leading example in modern warm gas thrusters is the 1U CubeSat High Impulse Propulsion System, or CHIPS, designed by VACCO and CU Aerospace. By imparting heat to the propellant by means of a heated cartridge located just before the nozzle, CHIPS can deliver significantly increased performance on an on-demand basis, but at a steep cost in power consumption. CHIPS is also notable because its total delivered impulse was proven to enable new suites of rendezvous, altitude change, and formation flying CubeSat missions [3]. Below is a table summarizing the key performance metrics of the MiPS cold gas thruster and the CHIPS warm gas thruster.

Table 2: Cold and Warm Gas Performance Summary

Parameter	MiPS	CHIPS
$\bar{I_{sp}}$	40	66
I_{tot}	250 N-sec	471 N-sec
Heater Power	5 W	25 W

As illustrated by Table 2, CHIPS significantly outperforms its cold gas counterpart in both total delivered impulse and overall specific impulse, and this is enabled by increasing the temperature of the exiting propellant while maintaining a similar propellant loading. This effect arises from the fact that the specific impulse of the thruster is proportional to the square root of the propellant temperature at the nozzle exit, as shown in Equation 1.

$$I_{sp} = M_e \sqrt{\gamma R T_e} \tag{1}$$

The exit mach number, M_e, is fixed for choked flow by the nozzle geometry, and since the specific heat ratio γ and gas constant R are fixed by the propellant choice, this leaves the exiting propellant temperature as the remaining available variable in determining the specific impulse of these systems. Since specific impulse represents the total impulse delivered by a given mass of propellant, the warm gas CHIPS system is subsequently able to deliver more impulse over its lifecycle compared to its cold gas equivalent.

However, as seen in Table 2, CHIPS also requires 400% more power than MiPS. It is noted that the heater power required by the MiPS module is nonzero because the bulk propellant storage vessel is kept within in an operating range of 0-60 ^oC. CubeSats are often power-limited due to their size, and since the priority of these satellites lies in the functionality of their payloads, it is in the interest of the mission to minimize the power that needs to be allotted to the propulsion system.

This project aimed to design a warm gas thruster that delivers mission-enabling total impulse comparable to the CHIPS warm gas thruster under the same power, volume, and propellant constraints as the MiPS cold gas thruster.

Canada's CanX-4 and CanX-5 missions provide a real-life benchmark for mission-enabling performance [4], so this propulsion system was also designed to meet the requirements of their underlying formation flying algorithm. For these missions, the CubeSats flew in five configurations with distances as low as 50 meters separating them. These missions are enabled by the FIONA formation flying algorithm, which requires a maximum single-maneuver impulse of 40 mN-sec and a mean time between maneuvers of 8 minutes and 40 seconds. This time between maneuvers allows a lower-power system to heat the requisite quantity of gas for a single maneuver to high temperatures, thereby increasing the thruster efficiency.

The design goals for this project are summarized in Table 3, synthesizing the constraints from MiPS, the performance parameters from CHIPS, and the propulsion requirements of the CanX missions.

Table 3: System design requirements.

Parameter	Target Value	Constraint Source
System Volume	$\leq$ 792.1 cm^3	[2]
Blowdown Impulse	$\geq$ 40 mN-sec	[4]
Total Impulse	$\geq$ 471 N-sec	[3]
Time Between Burns	$\leq$ 520 sec	[4]
Heater Power	$\leq$ 5 W	[2]

Designing a system that meets these requirements would provide all of the benefits of warm gas thrusters while utilizing 80% less power, allowing CubeSat missions to either greatly reduce onboard power requirements or increase the power available to their payloads, while also enabling complex formation flying missions.

2 Ideal System Design

First, an "ideal" propulsion system was designed. This system is ideal in the sense that while it is constrained to the total volume of a standard 1U CubeSat propulsion system, it also utilizes components that are not available for use within a standard senior design project. This assumption includes components such as the VACCO manifold, which integrates all electronics and fluid routing from the bulk storage tank to the nozzles, and all components based on VACCO ChEMS^{TM} modules such as isolation valves. These specialized components are required to fit within a realistic volume, but are also proprietary and are thus reverse-engineering these components is beyond the scope of this project.

The ideal system is intended to satisfy the performance parameters and constraints listed above. This will be done by taking advantage of the periodic nature of maneuvers in formation flying missions to only heat the propellant required for a single impulse at a time. The design centers around a small, intermediate vessel nested within the bulk propellant storage tank. The P&ID for the ideal system is shown in Figure 1:

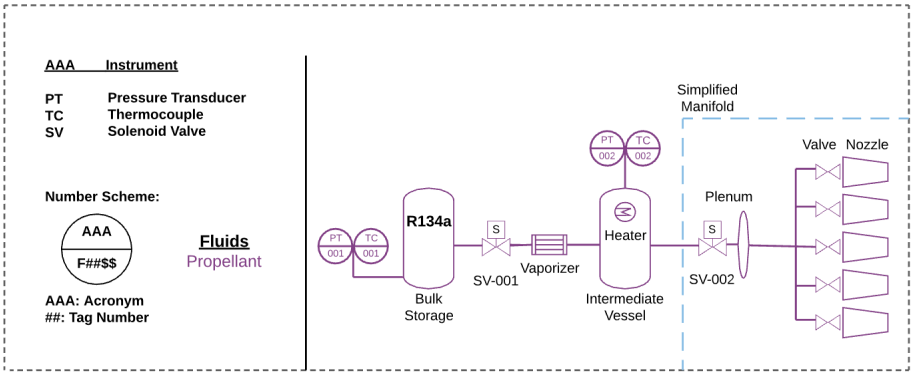

Figure 1: Ideal system Piping and Instrumentation Diagram (P&ID).

For each operation, the requisite quantity of propellant will be vaporized and stored within this intermediate tank. Then, nichrome heating elements surrounding the intermediate tank will raise the temperature of the propellant. Once the temperature meets the target value, the superheated gas is discharged from the intermediate vessel for expulsion through the thruster nozzles.

2.1 Methods and Approach

2.1.1 Steady-State Analytical Model

The first phase of analysis required building an analytical steady-state thermal model to test whether 5 Watts of power was sufficient to significantly raise the propellant temperature in a reasonably sized, realistically insulated tank. A spherical tank geometry was chosen because a sphere is the most area-efficient way to enclose any given volume, and minimizing thermal losses from the surface of the tank is a priority. Given this geometry and its uniform boundary conditions due to its positioning within the bulk storage tank, which is treated as an infinite thermal reservoir, a radial slice can be examined:

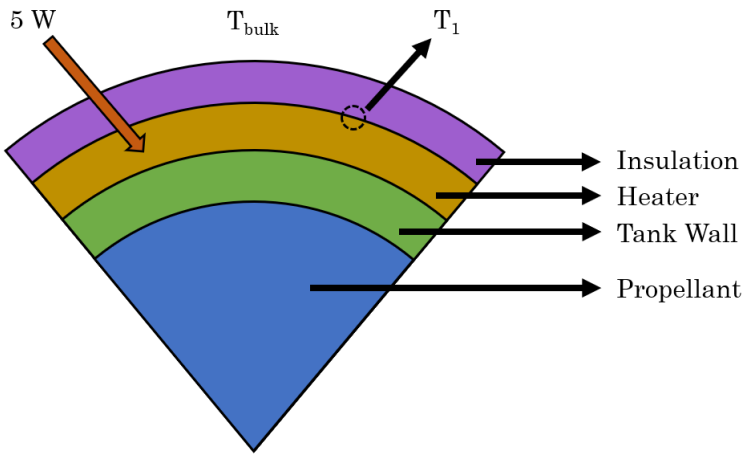

Figure 2: Lumped capacitance steady-state thermal model.

In this model, the propellant, tank wall, and heater are assumed to be isothermal during the heating process; this is intuitive because the heater power input is small, so the propellant and tank wall will wick the heat away before the heating element can become hotter than the two other layers. By assuming that conduction is the primary mode of heat transfer, the combined temperature of the three internal layers (T_1 in Figure 2) is related to heater input power, bulk storage temperature, tank geometry, and material properties by the following equation:

$$\dot{Q}_{out} = \frac{4\pi k_{ins} r_{in} r_{out} (T_{sys} - T_{env})}{t_{ins}} \tag{2}$$

From Equation 2 it is clear that to enable a high heated propellant temperature, an ideal insulation material would have a small thermal conductivity, low density, and a high operating temperature.

The strong dependence of the conduction equations at the core of the steady-state and transient models on insulation thermal conductivity led to the choice of aerogel for the intermediate tank insulation. Thermablok aerogel has an extremely low thermal conductivity of 0.015 W/m-k, a high maximum operating temperature of 650° C, and an extensive track record in aerospace applications [5].

It must be emphasized that these preliminary results were based upon geometries that visually seemed appropriate. As an example calculation, consider a setup with $\dot{Q}_{out} = 5$ W, $k_{ins} = 0.015$ W/m-k, $r_{in} = 0.02$ m, $r_{out} = 0.020508$ m, $T_{env} = 0$ C, and $t_{ins} = 0.005$ m. In this plausible configuration, the expected lumped system temperature is 989 C, which is significant enough to merit further system design and analysis. Note that the analytical steady-state model does not include heat lost through the connectors, as it was purely meant to serve as a first indication of feasibility, and thus it is expected that the results produced by this model will differ significantly from the more complex NX steady-state model presented in Section 2.1.4.

This steady-state model allowed us to get a preliminary estimate for the temperatures attained for various tank and insulation geometries within the input power limitations of the VACCO MiPS. However, this does not determine whether a system configuration meets the heat-up time requirement imposed by the formation flying algorithm of the CanX-4 and CanX-5 missions [4]. For this, a higher-fidelity transient model was developed to capture time-dependent behavior of the system.

2.1.2 MATLAB Transient Model

The FIONA formation flying algorithm requires propulsion systems to be able to perform single maneuvers, on average, every 520 seconds [4]. The thruster performance code, detailed in Section 2.1.3, determined that full intermediate vessel blowdowns take approximately one second, so 519 seconds were allocated for heat-up. The model works by calculating thermal losses by a variety of mechanisms at each timestep, subtracting this lost thermal power from the input power from the heater, then using the remainder to update the temperatures of system components. The two heat loss pathways are through the spherical insulation shell, via Equation 2, and by conduction through the metal connectors running from the intermediate tank through the insulation, which is governed by:

$$\dot{Q}_{out} = \frac{\pi k_{con} \left(r_{out}^2 - r_{in}^2\right) \left(T_{sys} - T_{env}\right)}{L_{con}} \tag{3}$$

The temperature rise in this lumped system for a given net thermal power input is determined by calculating a lumped heat capacity through the rule of mixtures:

$$C_{p,mix} = \sum_i \frac{m_i}{m_{mix}} C_{p,i} \tag{4}$$

Running this for a series of time steps produces a transient heating behavior of the system. It is noted that in this model, similar to the steady state model, the propellant, intermediate vessel, and heater are assumed to be isothermal.

Because temperature gradients are prohibited from forming in each layer of the system due to this isothermal assumption between the propellant, tank, and heater, the propellant

will take longer to heat up in reality, so this transient model was anticipated to produce slightly higher final heated propellant temperatures than node-based analyses. However, this transient model was still instrumental in capturing the bulk of transient heating behavior. It was also able to validate our assumption of the bulk propellant storage acting as an infinite thermal reservoir, as after calculating the heat that left the intermediate vessel into the reservoir over the course of a heat-up period, it was found that the bulk propellant temperature only saw a temperature increase on the order of a degree.

2.1.3 Time-Dependent Thruster Performance Simulation Code

Due to the time-dependent propellant pressures and temperatures inherent to blowdown systems, a simulation code was developed to track the performance of the thruster over the duration of a burn. The overarching code structure is presented in Figure 3.

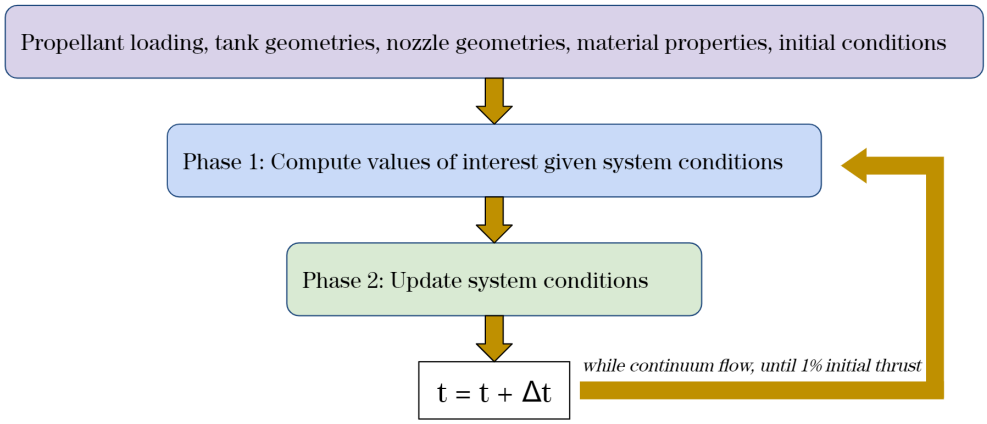

Figure 3: High-level structure of thruster performance simulation code.

The initial state of the propellant, as well as the geometry of the system, are fixed by the input initial conditions. Then, in Phase 1, a variety of parameters of interest are calculated given the system conditions at that first timestep. First, the Reynolds number is calculated at the throat:

$$Re = \frac{\rho^* u^* D_t}{\mu} \tag{5}$$

Isentropic nozzle flow relations, omitted here for brevity, are used to calcualte ρ^* and v^* in Equation 5. This Reynolds number will prove useful in multiple ways, the first of which is calculating the Knudsen number at the throat:

$$Kn = Re^{-1}\sqrt{\frac{\gamma\pi}{2}} \tag{6}$$

This parameter is crucial to verifying that continuum flow exists at the throat, which is set as a required condition for the duration of burns; if $Kn < 0.01$, then the thruster is still operating in this flow regime. Then, the Reynolds number is used to calculate the nozzle discharge coefficient, which will prove crucial to the thrust output of the system through Equations 8 and 9. Calculating the discharge coefficient in a micronozzle requires going

beyond standard equations; an experimentally-derived relation to Reynolds number, nozzle geometry, and a strongly nonlinear function of propellant specific heat ratio $f(\gamma)$ was used whose definition has been omitted here for brevity [6]:

$$C_d = 1 - (\frac{r_e}{r_t})^{1/4}(\frac{1}{Re})^{0.5} f(\gamma) \tag{7}$$

Here, r_e and r_t are the radii of curvature of the nozzle at the exit and throat, respectively.

With the discharge coefficient calculated through Equation 7, the mass flowrate $\dot{m}$ through the thruster can be calculated by:

$$\dot{m} = C_d D_t P_{tank} \gamma \sqrt{\frac{(\frac{2}{\gamma+1})^{\frac{\gamma+1}{\gamma-1}}}{\gamma R T_{tank}}} \tag{8}$$

Once the initial mass flowrate through the system is calculated by Equation 8, the primary performance metrics of interest, thrust and specific impulse, can be calculated. Assuming vacuum operation, thrust is determined by:

$$F_T = \lambda \dot{m} u_e + P_e A_e \tag{9}$$

where λ is a knockdown factor stemming from the inefficiency of the conical nozzle geometry. Finally, utilizing the results of Equations 8 and 9, the initial specific impulse of the system is calculated by:

$$I_{sp} = \frac{F_t}{g_E \dot{m}} \tag{10}$$

With these values of interest calculated, the code then updates the system conditions based on flow conditions and a series of assumptions. First, the number of moles of propellant are updated by the following intuitive relation:

$$n_{t+1} = \frac{\dot{m} \Delta t}{M} \tag{11}$$

An updated propellant density is calculated from Equation 11, which allows the code to update the intermediate vessel pressure:

$$P_{t+1} = (\frac{\rho_{t+1}}{\rho_t})^{\gamma} \tag{12}$$

assuming isentropic flow from the tank and ideal gas conditions. Finally, with the new density from Equation 11, the temperature in the intermediate vessel is updated by:

$$T_{t+1} = T_t (\frac{\rho_{t+1}}{\rho_t})^{\gamma-1} - \frac{k_{ins} A_{int} \Delta T \Delta t}{nLmC_v} \tag{13}$$

The first term in Equation 13 is the contribution from isentropic and ideal gas flow relations, and the second term takes into account the thermal soak from the intermediate vessel to the surrounding bulk storage tank through its insulation layer.

At this point, the code moves on to the next timestep of simulation, circling back to Phase 1 with the updated system parameters. This cycle continues until either the flow breaks the continuum regime dictated by the Knudsen number, or the thrust calculated by Equation 9 drops below 1% of the initial value. This cutoff was chosen because in practice, the continuum flow requirement is met well past the "useful" portion of the burn where the output thrust becomes minuscule. So, it was found that choosing to cut off the thruster at 1% of its initial thrust produced impacts on total system delivered impulse and performance that will realistically be lost in the startup and shutdown transients in practice.

All code for this thruster performance simulation is included in the appendix.

2.1.4 System Configuration Optimization

The thruster performance code in the previous section provided the capability to analyze the performance of any system configuration; setting the intermediate tank volume and insulation thickness fully constraints the system, because the manifold block is constant and the bulk storage tank encompasses the remaining system volume. In addition, since the intermediate tank is nested within the bulk storage tank, the bulk propellant volume is inversely proportional to the intermediate tank size. Thus, by sweeping the intermediate tank volume and insulation thickness, a global system optimization is performed.

First, wide ranges of sweep parameters are set, each spanning an order of magnitude or more. Next, the blowdown impulse (I_{blow}) and total impulse (I_{tot}) are computed for each configuration. The sizing trade is visualized in Figure 6. Next, viable configurations are extracted by filtering for solutions that yield $I_{blow} \geq 40$ mN-sec, per Table 3. Within the context of the sample experimental CubeSat missions, namely the CanX-4 and CanX-5 formation flying missions, there is no immediate benefit to having more than 40 mN-sec of blowdown impulse available. Thus, the optimal configuration is the configuration that meets the blowdown impulse requirement and has the highest total impulse to enable longer duration missions. The code for this optimization can be found in the Appendix.

2.1.5 Siemens NX Thermal Model

The target configuration determined by the optimization sweep of the performance code was ultimately based on the MATLAB thermal model, which encapsulates the bulk of the transient behavior of the system but ultimately makes certain assumptions that slightly distance the results from reality. So, a node-based thermal model was developed in NX to test how accurate these assumptions were, and when discrepancies in system behavior inevitably arise, this also enabled the fine-tuning of the insulation thickness to hit the desired target temperature.

This model was comprised of three concentric spherical shells, each with a custom material assignment implementing the same material properties found in the MATLAB simulation in order to most directly validate the MATLAB model. Starting from the outside, these layers are the insulation, a combined heater and intermediate vessel wall, and the propellant. 316L stainless steel inserts will provide fluid transfer pathways connecting the forward and aft ports to the intermediate tank volume. A summary of the simulation configuration, including surface contacts, thermal constraints, and meshed zones, is presented in Figure 4.

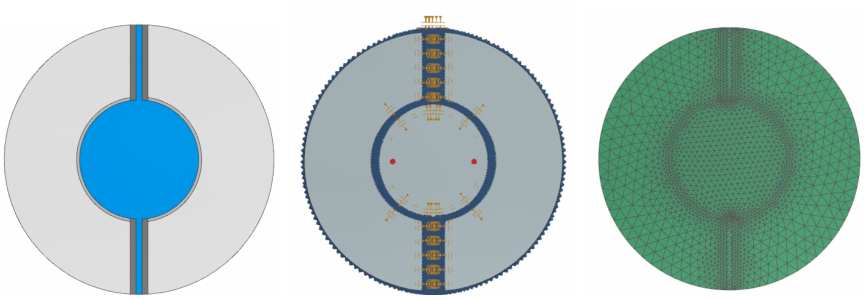

Figure 4: From left to right: NX simulation model cross section, model contacts and heat transfer pathways, and cross-sectional view of model meshes.

Perfect conduction is assumed between layers, and the mesh is tightened on the thin tank wall to ensure key behavior is adequately captured by the simulation. A boundary condition of 0° C is placed on the outside of the insulation, the outer sphere, in accord with the infinite thermal reservoir approximation for the bulk storage tank in which the intermediate tank is housed. This temperature is the bulk propellant storage temperature. A crucial improvement over the analytical steady state model is that this now takes into account the thermal effects of adding a second dimension to the pathways for energy loss, while the analytical model neglected these in favor of a purely one-dimensional heat transfer model. The heater power of 5 Watts is inputted as a volumetric heat generation within the combined heater and intermediate vessel wall volume, as it is assumed that all input power is deposited directly into the tank wall.

With this model set up, a transient simulation was then run and then compared against to the results found using MATLAB. Ultimately, this comparison will determine the finalized ideal system dimensions. A steady-state model was also developed to investigate system behavior in the event that the heater was unable to be turned off for an indefinite period of time.

2.1.6 Manifold and Line Sizing

The fluid pathways between the bulk storage and the intermediate vessel were sized, using VACCO's MiPS thruster design as a starting point and the mass flowrates determined by the nozzle performance code, in order to create a reasonable pressure drop across the system. Figure 5 below represents an approximated flow diagram of VACCO's MiPS propulsion manifold which supported the ideal system design.

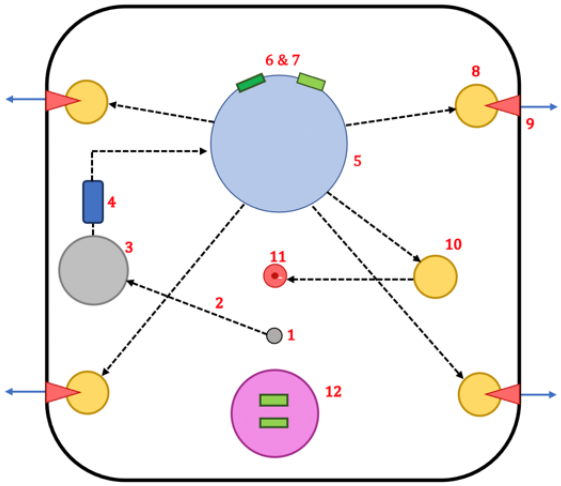

Number	Item
1	Fill Port
2	Conduit Lines (1.5 mm Diameter)
3	Isolation Valve
4	Particle Filter
5	Plenum
6	Thermocouple
7	Pressure Transducer
8	Tangential Thruster Valve (x4)
9	Tangential Thruster Nozzle (x4)
10	Axial Thruster Valve
11	Axial Thruster Nozzle (out of page)
12	Bulk Storage Thermocouple and Pressure Transducer

Figure 5: Approximate flow diagram of the VACCO MiPS manifold, from which the approximated manifold of this propulsion system was derived.

Given a maximum mass flow rate of $3.014{*}10^{-4}$ kg/s from the thrust performance calculations, the fluid properties at the target state were used in conjunction with Poiseuille's Equation to determine volumetric flow rate. From this, it was determined that 1-1.5 mm mm diameter conduits would be adequate for reasonable fluid transport from intermediate tank to each of the five nozzles. With these values, along with computed Reynolds number (≈ 500) and roughness ratio of the manifold (0.001), the Haaland formula, with $\approx 2\%$ error from the Moody Diagram, was used to determine the unitless friction factor of ≈ 0.01. This friction factor, f_D, is then used in the Darcy-Weisbach equation,

$$\Delta p = f_D \frac{\rho V^2}{2D} \tag{14}$$

to compute a pressure drop of the manifold conduits per unit length. This pressure drop was found to be negligible on the length scales of the manifold.

2.2 Results

The viable solutions produced by the parameter sweep detailed in Section 2.1.3 are shown in Figure 6:

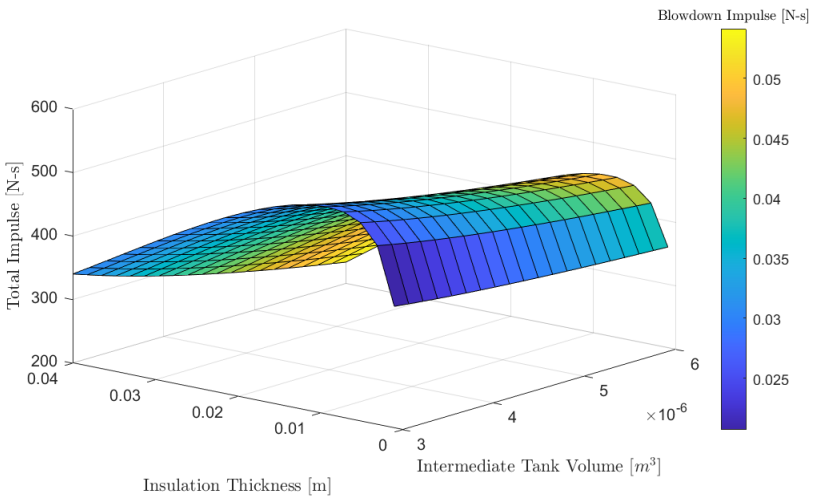

Figure 6: Total delivered impulse and blowdown impulse as a function of intermediate tank volume and insulation thickness.

The optimal configuration in Figure 6 is the point on the surface that has at least 40 mN-sec of blowdown impulse and the highest total impulse given this constraint. This configuration is summarized in Table 4:

Table 4: MATLAB-determined optimal intermediate tank and insulation parameters.

Design Parameter	Value
Intermediate Tank Volume	$4.42 * 10^{-6}$ m^3
Insulation Thickness	1.13 cm

With this geometry, the system delivers a total impulse of 478.5 N-sec with a single blowdown impulse of 40.0 mN-sec. Note that it is expected that the total delivered impulse will change when the required insulation thickness is refined with the NX thermal model, but the blowdown impulse will remain the same. This is because changing the insulation thickness will alter the available volume for propellant in the bulk storage tank, while the blowdown impulse will be practically unchanged with the same tank volume and slightly different insulation thickness due to the small effect of heat loss through the insulation over the course of a one-second blowdown; the system was designed to minimize thermal losses from the intermediate vessel, and over the course of a full blowdown, the energy lost from the heated vessel amounts to 0.00000075% of the energy ultimately used for propulsion.

While performance was not found to exhibit significant sensitivity to nozzle geometries around the considered design, which is constrained by the existing VACCO nozzle and manifold design upon which this system is originally based, these geometries are still important to a complete understanding of this propulsion system. Nozzle geometries can be seen in Figure 7.

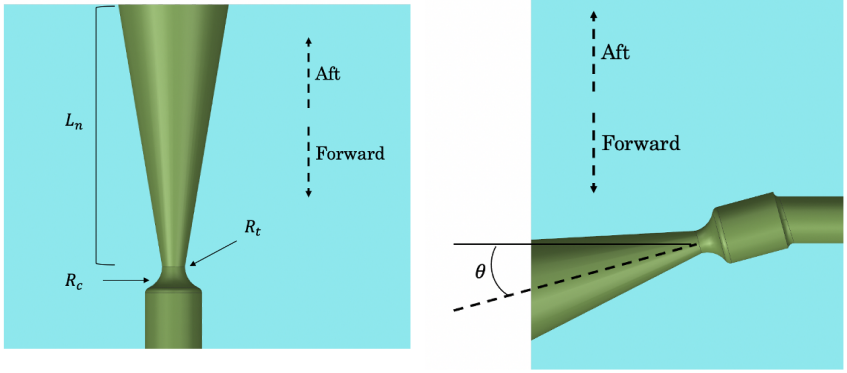

(a) Axial Nozzle

(b) Tangential Nozzle

Figure 7: The left image is a capture from CAD of the axial nozzle, with parameter call outs. The right image is of the tangential thruster which is directed away from the aft face of the craft by 15^o.

The important dimensions of the these nozzle geometries are the radius at the throat, the radius of curvature, and the length of the nozzle denoted by R_t, R_c, and L_n respectively. The values for these parameters can be seen in Table 5. Note that Figure 7(b) shows the orientation of the four tangential thrusters. Note that $\theta = 15°$ and represents the angle that the thruster central axis makes with the horizontal, and is different from the conical nozzle divergence half-angle. This slight angle gives the spacecraft the ability to produce a ΔV in the aft direction. This design was informed by the VACCO MiPS thruster [7].

Table 5: Nozzle parameters.

Parameter	Value
Throat Diameter (R_t)	0.4 mm
Converging Section Radius (R_c)	0.8 mm
Throat-to-Exit Length	4.572 mm
Divergence Angle	12°
Area Ratio	20
Knockdown Factor (λ)	0.989

Utilizing the thruster performance code discussed in Section 2.1.3, the time traces of various performance metrics and fluid properties over the course of a blowdown for the optimal configuration are shown in Figure 8:

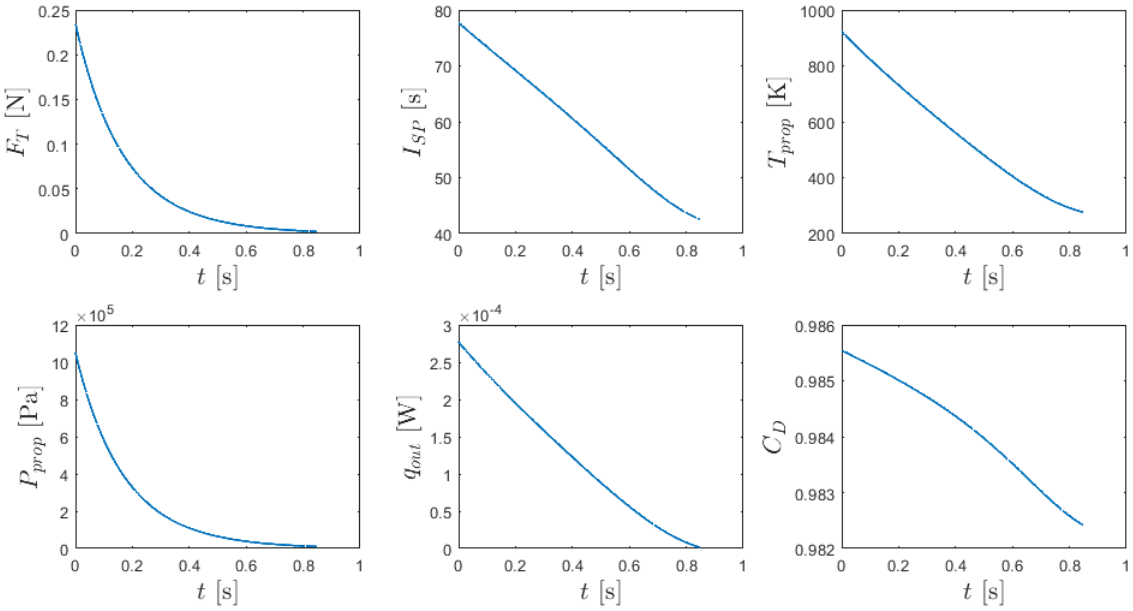

Figure 8: Thruster performance metrics and intermediate tank fluid properties as a function of time over the course of single blowdown of the intermediate vessel.

While the blowdown impulse and total impulse are displayed on Figure 6 and listed in Table 7, the weighted specific impulse ($\bar{I_{sp}}$) and average thrust ($\bar{F_T}$) are computed via the curves shown in Figure 8. The weighted specific impulse is weighted according to the thrust time trace, meaning the system I_{sp} early in the blowdown when the majority of the impulse is delivered is given more weight. For the optimal configuration shown, $\bar{I_{sp}} = 68.2$ sec and $\bar{F_T} = 42.7$ mN.

The tank heat-up profile and thermal losses over time produced by the MATLAB transient model for the optimal configuration presented in Table 4 are shown in Figure 9:

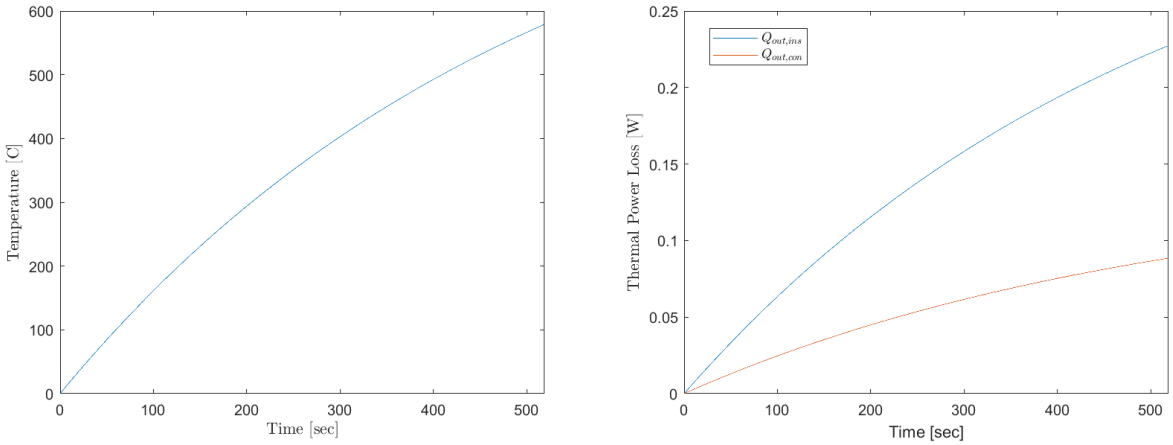

(a) (b)

Figure 9: Lumped system heat-up profile (a) and thermal losses through the insulation and connectors (b) in the optimal configuration detailed in Table 4

The validity of the lumped capacitance assumption implemented in the MATLAB transient code was tested by using the NX thermal model to produce a similar transient behavior. The simulation results with the MATLAB-produced insulation thickness yielded a propellant temperature of 547° C, a 5% difference from the MATLAB results. This small discrepancy demonstrates that the assumptions made in the MATLAB model were reasonably accurate. The insulation thickness was then adjusted to reach the desired maximum temperature after 519 seconds. The final intermediate tank and insulation parameters refined by the NX thermal model are presented in Table 6:

Table 6: Refined optimal intermediate tank and insulation parameters.

Design Parameter	Value
Intermediate Tank Volume	$4.42 * 10^{-6}$ m^3
Insulation Thickness	1.21 cm

The corrected NX transient thermal model results after 519 seconds of heat-up time are presented in Figure 10:

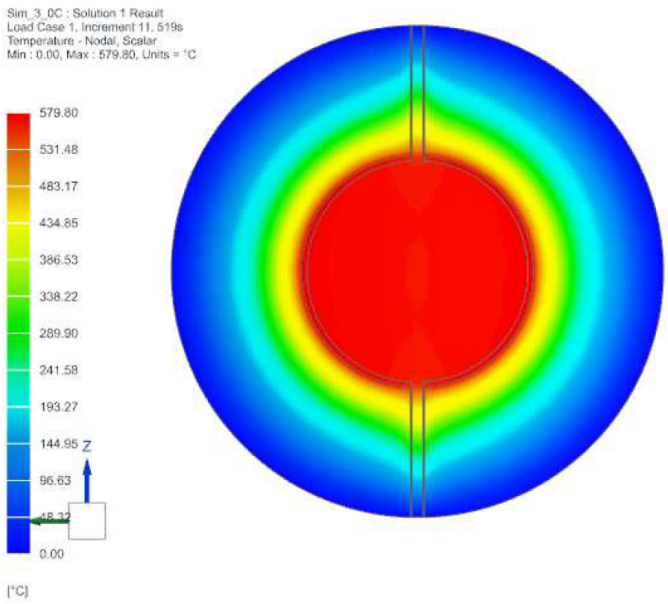

Figure 10: NX thermal transient model state after 519 seconds of heat-up time with the refined insulation thickness. Note that the propellant reaches the target temperature of 579° C.

As expected, thermal gradients formed around the metal connectors leaving and entering the tank as they pulled heat along their axes. The steady-state behavior of the refined system was also explored with the NX thermal simulation environment. The steady-state behavior of the heated tank is shown in Figure 11:

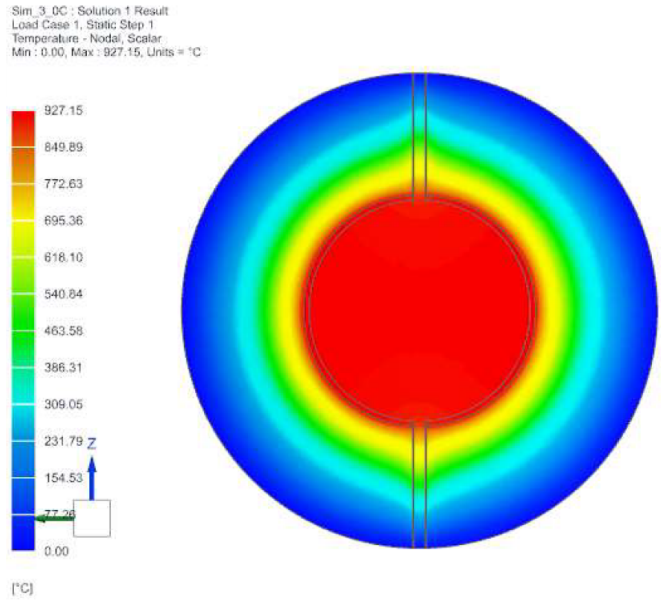

Figure 11: NX thermal model steady-state behavior with the refined insulation thickness. Note that the propellant exceeds the insulation maximum operating temperature of 650° C, requiring a failsafe in the event of a loss of heater control.

With all components finalized, the final CAD model was generated using Siemens NX. This model is displayed at the end of the assembly process shown in Figure 13, and a cross-section view of this configuration is shown in Figure 12:

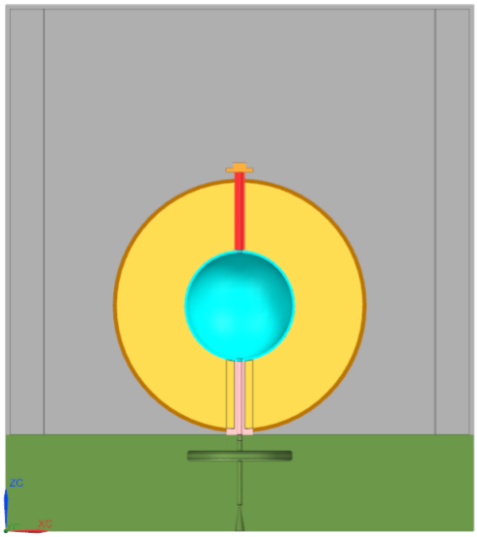

Component	Color
Intermediate Tank	Cyan
Forward Connector	Red
Aft Connector	Pink
Insulation	Yellow
Insulation Shield	Brown
Vaporizer + Valve	Orange
Manifold	Green
Bulk Storage Tank	Grey

Figure 12: Cross-section view of optimized ideal propulsion system.

This model has a combination of off-the-shelf and custom parts. The bulk storage tank is custom-made to maximize internal volume while accommodating the standard CubeSat rails, and can be manufactured via conventional methods. Another custom part is the intermediate tank, which is created by joining two thin hemispheres of 316L stainless steel together via a circumferential weld. This stainless steel was chosen for its mechanical properties at the temperatures seen in this application. The intermediate vessel thickness was sized via thin-walled pressure vessel calculations with a factor of safety of 1.2. Surrounding the intermediate tank is the insulation shell made from Thermablok aerogel and an insulation shield made from Al-6061. Both of these are custom parts and the insulation shield is manufactured using the same method as the spherical intermediate tank. The connectors leading into and out of the intermediate vessel are cut from off-the-shelf 316L stainless steel tubing with outer diameter 0.050" and inner diameter 0.042". The manifold is designed and manufactured by VACCO for its propulsion systems using proprietary ChEMS modules. The vaporizer and the valve in located in the bulk storage tank are also purchased from VACCO because they use the same proprietary technology. The CAD model excludes the thin heating element and wiring, although these omissions do not alter the following assembly process.

The assembly process for the propulsion system is presented in Figure 13.

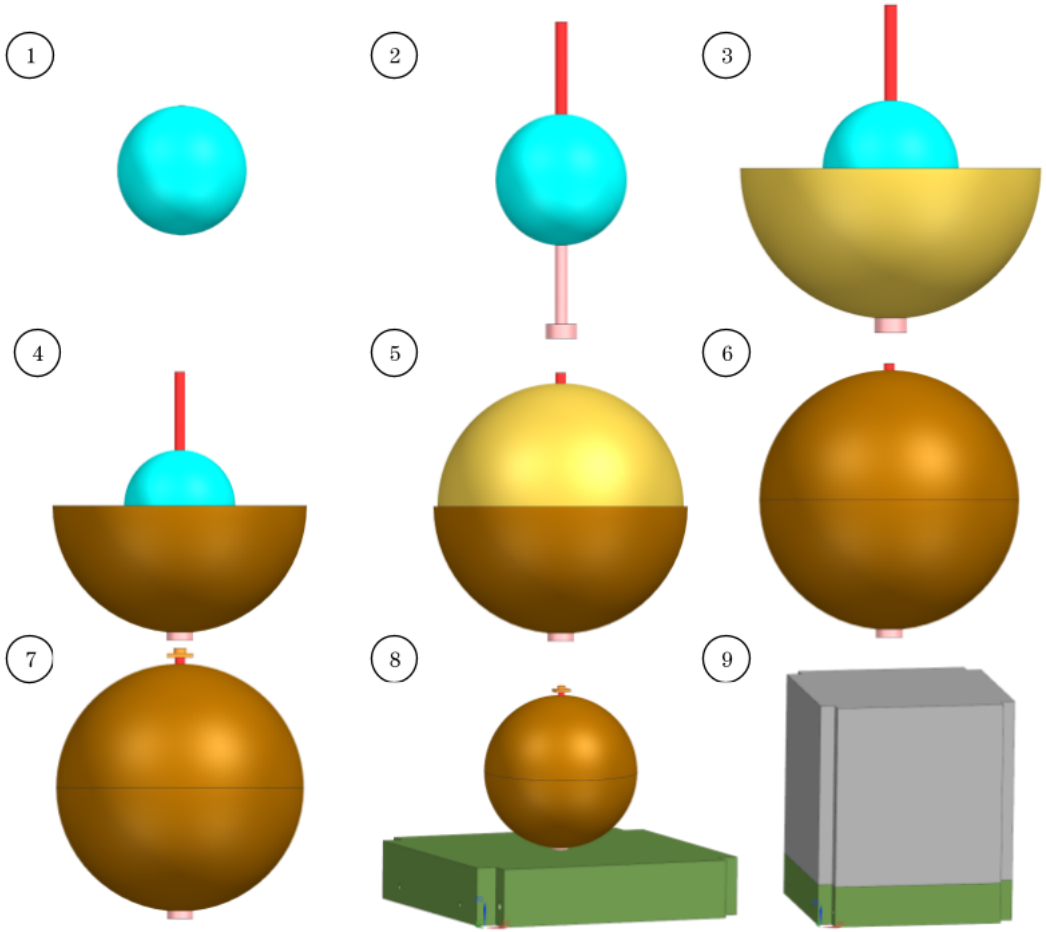

Step	Description
1	The two hemispheres are joined via circumferential weld
2	The forward and aft connectors are attached to the intermediate tank via circumferential edge weld.
3	The lower hemisphere of insulation is fitted around the aft connector. Note that the wider section of the aft connector introduces the need for a third small, cylindrical insulation piece that hugs the narrow part of the connector
4	The bottom bulk shell is fitted around the insulation and aft connector. The bottom shell circumferential edge welded to the aft connector.
5	The upper hemisphere of insulation is added around the forward connector.
6	The upper half of the bulk shell is attached to the bottom half of the bulk shell and to the forward connector via circumferential welds.
7	The vaporizer and valve volumes are added to the extended forward connector via a pipe fitting.
8	The sub-assembly of the intermediate tank and surrounding components is left separate from the manifold until this step to make accessing it easier. The head of the aft connector is circumferentially welded to manifold.
9	The bulk storage tank is attached to the manifold via a circumferential weld and the propulsion system is ready to be tested.

Figure 13: Assembly Process Diagram. These nine steps show the order of operations to build the propulsion system.

The system was designed such that any components added to the existing MiPS architecture are conventionally manufacturable and mandate simple additional assembly steps. It is noted that fill and drain operations are conducted through the axial nozzle, consistent with the procedures of the VACCO MiPS system [7].

2.3 Discussion

The performance of the refined optimal system is compared against the original design constraints (Table 3) in Table 7:

Table 7: System design requirements and current values.

Parameter	Target Value	Design Value	Constraint Source
System Volume	$\leq$ 792.1 cm^3	792.1 cm^3	[2]
Blowdown Impulse	$\geq$ 40 mN-sec	40.0 mN-sec	[4]
Total Impulse	$\geq$ 471 N-sec	475.1 N-sec	[3]
Time Between Burns	$\leq$ 520 sec	520 sec	[4]
Heater Power	$\leq$ 5 W	5 W	[2]

The design summarized in Tables 6 and 7 achieved the original goal of mission-enabling performance under the same power, volume, and propellant constraints as an industry standard cold gas thruster. Figure 6 shows that a multitude of possible system configurations meet all of the design constraints described in Table 3 while delivering a total impulse comparable to the CHIPS thruster. However, since no more than 40 mN-sec single-burn impulse is required by the formation flying algorithms used in the CanX-4 and CanX-5 missions [4], the optimal system configuration is that which yields a blowdown impulse as close as possible to 40 mN-sec, subsequently maximizing the total delivered impulse. Visually, this is represented by the 40 mN-sec blowdown impulse solution lying on crest of the solution surface in Figure 6. This solution is how the optimal system parameters listed in Table 6 were determined.

As seen in Figure 8, the system thrust and intermediate vessel pressure decay rapidly with time, while specific impulse, propellant temperature, and heat lost from the intermediate vessel decay relatively linearly. This yields an impulse-weighted specific impulse approximately 15% higher than a temporally-averaged specific impulse, implying that most of the impulse delivered by the system is done so in its higher-efficiency regime. The nozzle discharge coefficient is relatively steady over the course of the burn despite the changing inlet conditions.

To truly optimize the system beyond its current state, the connector lengths can be increased beyond the insulation to reduce thermal losses and thus allow for higher propellant temperatures. However, the performance gains are negligible (0.5%/cm added length) at a cost of significant additional assembly complexity; once the connector length extends beyond the insulation, the intermediate vessel assembly must then be supported off of the manifold during the assembly process.

Figure 10 shows that the selected configuration behaves as expected, and reaches the target temperature after 519 seconds of heat-up time. Figure 11 shows that in the scenario where the heater remains locked in the on position, the steady-state temperature reached by the heater is above the maximum operating temperature of the insulation [5]. Thus, failsafes must be designed to ensure that the circuit is broken in this event. Such a system would likely be comprised of foil-type thermocouples monitoring the surface temperature of the heater, and triggering a switch to break the circuit when the heater temperature exceeds the maximum operating temperature of the insulation.

Comparing Figures 9 and 10, the NX model produces a heat-up temperature that is 5% less than the temperature predicted by the MATLAB model. This discrepancy is due to the fact that the analytical conduction model assumes that the heater, intermediate vessel, and its contained propellant are collectively isothermal during heating. Since the NX model does not make this assumption, allowing for the formation of temperature gradients over the intermediate vessel walls and through the contained propellant, it is expected that the increased fidelity within the NX model should result in an overall lower temperature reached at the heater-insulation boundary.

3 Brassboard System Design

Once the ideal design of the propulsion system was finalized, a brassboard version was designed to test its key thermal and performance-related behavior over the course of a blowdown in a realistic laboratory environment. This system relaxed the prior 1U volume constraint, but also requires all components to be feasibly obtained and tested in a standard senior design project.

3.1 Thermal Considerations

To produce meaningfully comparable behavior, it is imperative that all key thermal environments remain similar across the ideal and brassboard designs. The first subsystem with key thermal considerations is the intermediate tank. Given that the brassboard system operates at room temperature (25° C) instead of the ideal system environment (0° C), the insulation thickness must be altered to allow for the same thermal losses. This change is compounded by the fact that the brassboard system uses 1/8" 316L stainless steel tubing for the connectors leading into and out of the intermediate tank, which results in a significantly larger heat transfer area than the thin-walled connectors in the ideal system and thus results in a lower maximum temperature at 519 seconds. However, the geometric constraints of the brassboard system confining it to a 1 ft by 1 ft plate also prevents the insulation from growing too large to accommodate these exacerbated losses through the connectors. To balance these considerations, the insulation thickness adjusted to the maximum value allowed by the brassboard geometry, and the heater power was increased to achieve the same heating profile in 519 seconds with the updated insulation thickness and connector thermal losses. The required heater power is 16.5 Watts, given the geometrically-constrained maximum insulation thickness of 1.136 cm. Note that this is different from the refined insulation thickness because it is solely set by the space available on the mounting plate.

The second key thermal consideration is the propellant heat loss as it passes through the manifold from the intermediate tank to the nozzle. In the ideal system analysis, the manifold is treated as an isothermal body held at the ambient temperature (0° C), which cools the propellant by 3% in the worst-case scenario. Thus, it was imperative that the tube acting as a manifold from the intermediate tank to the nozzle acted similarly isothermal at room temperature, and also yielded a similar drop in propellant temperature. Using the Dittus-Boelter relations for turbulent flow in smooth circular tubes, it was found that 1.5 inches of readily available 1/8" tubing could provide the same propellant temperature drop as expected in the ideal system manifold, while only raising the tube temperature by approximately 1%, preserving the isothermal assumption to an acceptable degree, while also providing no worse pressure drop than expected in the manifold. However, the isolation valve between the intermediate tank and the nozzle must be kept away from the intermediate tank to prevent excessive heating of the component. Since the valve itself is 1.9" long, and thus already provides the desired temperature drop if maintained at 25° C, some additional standoff tubing must be placed between the intermediate tank outlet and the valve, which will incur additional temperature drop in the propellant. By keeping the total temperature drop to 6%, an additional 1.3" of tube can be afforded before the valve, thereby providing a standoff to prevent excessive heating of the valve body.

3.2 Design

The P&ID of the brassboard system is presented in Figure 14.

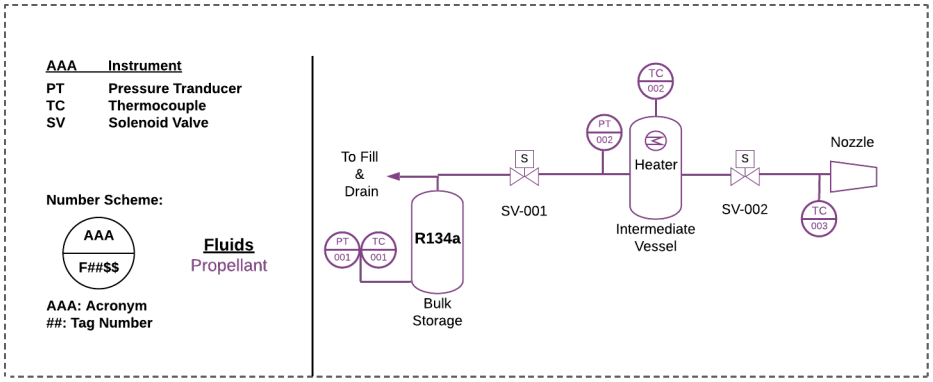

Figure 14: Brassboard system Piping and Instrumentation Diagram (P&ID).

To realize this P&ID in a bench-top setting, it was designed to mount to a 12"x12" plate in order to interface with an existing thrust stand. The final design of the brassboard system is presented in Figure 15.

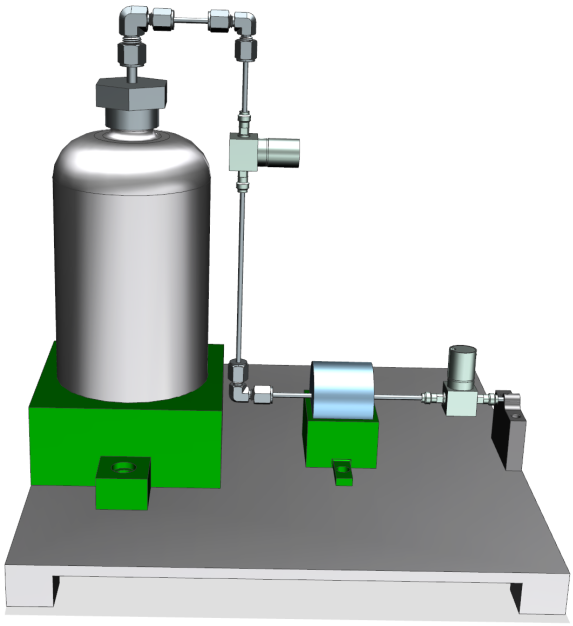

Figure 15: Brassboard system design overview.

Per Figure 14, pressurized R134a vapor is tapped off from the top of the bulk storage tank and fills the intermediate vessel when SV-001 is open and SV-002 is closed. SV-001 is then closed, isolating the gas within the intermediate vessel. The intermediate vessel is then heated by supplying power to the nichrome foil heater wrapping the tank until the target temperature is reached after 519 seconds. SV-002 is then opened, allowing the tank to blow down through the nozzle.

A complete Master Equipment List (MEL) and manufacturing drawings for custom components for the brassboard design are included in the appendix. An off-the-shelf bulk storage tank is mounted to the plate by a 3D-printed support structure, and is connected via 316 stainless steel tubing 1/8" to the intermediate tank with an in-line isolation valve. Note that since the bulk storage tank is now mounted in a fixed orientation and within a gravitational field, the vapor accumulating at the top of the tank can be directly siphoned off, negating the requirement for a vaporizer. The intermediate tank is no longer nested within the bulk storage tank, as the presence of the former was found to have negligible thermal effects on the latter, so the aluminum shell separating the insulation from the bulk propellant is no longer required. The intermediate tank and its insulation are mounted to the metal plate via a 3D-printed plastic cradle; the plastic will not melt because the surface of the insulation does not heat up significantly over the course of the propellant heating process. The outlet of the intermediate tank leads directly to another isolation valve, which is assumed to be a high-temperature variety of the valve presented for reference. This valve then allows propellant to flow into the tube length that acts as a thermally analogous manifold before reaching the nozzle and venting to vacuum conditions.

4 Conclusion

A staged warm gas thruster design is presented that provides mission-enabling total impulse, single-maneuver impulse, and inter-maneuver timing to accommodate the FIONA formation flying algorithm while staying within the stringent power, volume, and propellant type requirements of industry-standard cold gas thrusters. Subsequently, the project goal was achieved. The presented design outperforms the impulse delivered by the CHIPS propulsion system, which was proven to provide a mission-enabling amount of total impulse, while requiring only a fifth of the heating power. In addition, a brassboard version of this system is presented that can be manufactured and tested in-house at USC and mimics the thermal environment of the ideal spacecraft system. This propulsion system has extensive applications in the booming sphere of CubeSat-based missions, as this potentially enables a suite of more complex mission scenarios without increasing the power requirement currently acceptable to standard cold gas thrusters. Alternately, missions already based on the CHIPS module or similar warm gas thrusters could meet or exceed their current delivered impulse needs while either cutting their onboard power requirement by 80% or accommodating more robust onboard instrumentation packages.

References

[1] M. R. Firm, "Cubesat market," *Marketsandmarkets*, 2018.

[2] VACCO Industries, *Standard Micro Propulsion System Datasheet.* 2015, Online.

[3] N. J. Hejmanowski, C. A. Woodruff, R. Burton, D. L. Carroll, and A. D. Palla, "Cubesat high impulse propulsion system (chips) design and performance," *63rd JANNAF Propulsion Meeting*, 2016.

[4] G. Bonin, N. Roth, S. Armitage, J. Newman, B. Risi, and R. E. Zee, "Canx–4 and canx–5 precision formation flight: Mission accomplished!," *Conference on Small Satellites Proceedings*, 2015.

[5] T. Inc., "Thermablok aerogel insulation blanket datasheet." Online.

[6] N. M. Kuluva and G. A. Hosack, "Supersonic nozzle discharge coefficients at low reynolds numbers," *American Institute of Aeronautics and Astronautics*, 1970.

[7] J. Cardin, K. Coste, D. Williamson, and P. Gloyer, "A cold gas micro-propulsion system for cubesats." Presentation slides from the 17th Annual AIAA/USU Conference on Small Satellites.

Appendix

Thruster Performance Code

Main Performance Code

```
function [projected_total_impulse, blowdown_impulse, P_0,
 percent_left,...
    weighted_Isp, mean_thrust] = nozzle_perf(T,m_prop,D_t, V,
 L,M_exit,...
    V_allowed, rat,lambda)

%Goal: calculate evolution of nozzle performance over entire burn
 time.
%Starting parameters: T,P,n in intermediate tank, also nozzle geometry
%For each timestep, assume T,P are constant and go into nozzle.
 Calculate
%Nozzle performance (thrust, Isp). Then, calculate the m_dot, and for
 some
%chosen delta_t, remove that mass of gas from the intermediate tank
 and
%update the T,P, and n in the intermediate tank accordingly (blowdown)
%Rinse and repeat for entire burn. Performance should drop off over
 time.

%%%% Define Constants %%%%
R_uni = 8.314; % [J/K-mol]
rho_prop = 1295.1; % R134a liquid density @0deg C [kg/m^3]

%%%% Initial Conditions in the Intermediary Tank   %%%%
M=102.03/1000; %molar mass of propellant [kg/mol]
n=m_prop/M; %starting moles of propellant
k=1.20; %for R134a
R=R_uni/M; %propellant-specific gas constant

%%%% Nozzle Characteristics %%%%
u = 14.5*10^-6; %[kg/m*s], dynamic viscosity
gamma=k; % rename specific heat ratio for later use
f_gamma = 0.97 + (0.86 * gamma);% approx.
r_ratio = 2; %[], this value comes from the Figures 2/3 of the paper
r_t = D_t/2; %[m], radius of the throat
r_c = r_t * r_ratio; %[m],radius of curvature leading to the throat
L_connector = L; % reset

%%%% Insulation Characteristics %%%%
k_ins = 0.015; % thermal conductivity [W/m-k]
r_sphere = (3*V/(4*pi))^(1/3); % sphere radius
A_sphere = 4*pi*r_sphere^2; % sphere surface area
T_bulk = 273.15; % bulk storage temp [K]

%%%% Compute Initial Pressure %%%%
P = (n*R_uni*T) / V;
P_0 = P;

%%%% Discretize Time %%%%
delta_t=0.0001;

%%%% Initialize Loop Variables %%%%
```

Main Performance Code

```
i=1;
continue_flag=true;

%%%% Primary Loop %%%%
while (continue_flag == true)

    time_vec(i) = delta_t * (i-1); % update time vector

    % compute throat conditions
    Tstar=T*((gamma+1)/2)^(-1); % throat temperature
    rhostar=(m_prop/V)*((gamma+1)/2)^(-1/(gamma-1)); % throat density
    v = sqrt(gamma * R * Tstar); % throat velocity is sonic
    Re_calc = (rhostar*v*D_t)/u; % Reynolds number at throat
    Kn_vec(i)=(1/Re_calc)*sqrt(gamma*pi/2); % Knudsen number at throat
    % Cd computed from paper on micronozzles
    Cd_vec(i) = ((r_c + (0.05*r_t))/(r_c + (0.75*r_t)))^0.019 * ...
        (1-((r_c + (0.1*r_t))/r_t)^0.21 * (1/Re_calc)^.5 * f_gamma);
    mdot=mdot_calc(P, T, k, D_t, R, Cd_vec(i)); % mass flow rate
    mdot_vec(i)=mdot; % update mass flow rate vector

    % compute performance metrics
    v_e=exit_velocity_calc(T,R,k,M_exit); % exit velocity
    ue_vec(i)=v_e; % update exit velocity vector

 thrust_vec(i)=thrust_calc(mdot,v_e,lambda,P,M_exit,gamma,D_t,rat); %
 compute thrust
    isp_vec(i)=isp_calc(thrust_vec(i),mdot); % compute specific
 impulse

    % update propellant properties based on that amount of propellant
    % leaving the intermediate tank
    n=update_n(n,mdot,delta_t,M); % compute number of moles of gas in
 tank
    n_vec(i)=n; % update remaining moles vector
    P=update_P(P,V,n,k,mdot,delta_t,M); % compute updated tank
 pressure
    P_vec(i)=P; % update pressure vector
    % compute new tank gas temp based on blowdown + heat losses
    [T,q_lost(i)]=update_T(T,V,n,k,mdot,delta_t,M,T_bulk,k_ins,...
        A_sphere,L,R);
    T_vec(i)=T; % update tank gas temperature vector
    % if thrust is <1% max, end loop
    if i>1 && (isnan(thrust_vec(i)) ||
 thrust_vec(i)<0.01*thrust_vec(1))
        continue_flag = false;
    end
    i=i+1; % otherwise, add another slot to the vectors
end

% compute percentage of remaining moles of propellant after end of
 burn
percent_left=100*n_vec(length(n_vec))/n_vec(1);

%%%% Plotting %%%%
```

Main Performance Code

```
%{
setsize=16;

subplot(3,3,1)
plot(time_vec,thrust_vec,'linewidth',1.5);
xlabel('$t$ [s]', 'Interpreter', 'latex','fontsize',setsize);
ylabel('$F_T$ [N]','Interpreter','latex','fontsize',setsize);

subplot(3,3,2)
plot(time_vec,isp_vec,'linewidth',1.5);
xlabel('$t$ [s]', 'Interpreter', 'latex','fontsize',setsize);
ylabel('$I_{SP}$ [s]','Interpreter','latex','fontsize',setsize);

subplot(3,3,3)
plot(time_vec,T_vec,'linewidth',1.5);
xlabel('$t$ [s]', 'Interpreter', 'latex','fontsize',setsize);
ylabel('$T_{prop}$ [K]','Interpreter','latex','fontsize',setsize);

subplot(3,3,4)
plot(time_vec,P_vec,'linewidth',1.5);
xlabel('$t$ [s]', 'Interpreter', 'latex','fontsize',setsize);
ylabel('$P_{prop}$ [Pa]','Interpreter','latex','fontsize',setsize);

subplot(3,3,5)
plot(time_vec, q_lost,'linewidth',1.5);
xlabel('$t$ [s]', 'Interpreter', 'latex','fontsize',setsize);
ylabel('$q_{out}$ [W]', 'Interpreter', 'latex','fontsize',setsize);


subplot(3,3,6)
plot(time_vec, Cd_vec,'linewidth',1.5);
xlabel('$t$ [s]', 'Interpreter', 'latex','fontsize',setsize);
ylabel('$C_D$', 'Interpreter', 'latex','fontsize',setsize);

%}

%%%% Burn Impulse and Mass %%%%

burn_impulse = trapz(time_vec,thrust_vec); %impluse from burn, [N-s]
burn_mass = trapz(time_vec, mdot_vec); % mass expelled during burn
 [kg]

%%%% Determine Ratio of Lost to Used Energy %%%%
lost_energy = trapz(time_vec,q_lost); %total lost (unusable) energy

m_vec=n_vec*R;
intermed=0.5*ue_vec.^2;

used_energy=trapz(flip(m_vec),intermed);

%%%% Output to Mesh Plot %%%%
% static volumes to remove from consideration
Vol_rails = 1.6735e-5; % volume of rails
Vol_bulk_shell = 2.77e-5; % volume of bulk storage tank shell
```

```
vol_vaporizer = 4.91e-9; % volume of the vaporizer
vol_valve = 1.13e-8; % volume of the chEMS isolation valve
Vol_manifold = 1.45e-4; % volume of nozzle/electronics manifold
system_vol = 0.089*.089*.1; % total system volume
vol_tube_stub = 3.14159e-9; % volume of tube stub from insulation
 shell

% compute volume of metal shell around insulation
r_ins = (3*V_allowed/(4*pi))^(1/3);
t_shell = 0.000762; % thickness of shell (0.03") [m]
vol_ins_shell = 4*pi*((r_ins + t_shell)^3 - r_ins^3)/3;

% compute maximum remaining volume for propellant
max_bulk_prop_vol = system_vol - Vol_rails - Vol_bulk_shell -
 Vol_manifold  - ...
    V_allowed - vol_vaporizer - vol_valve - vol_ins_shell - ...
    vol_tube_stub;
bulk_prop_mass = max_bulk_prop_vol * rho_prop; % bulk prop mass [kg]

blowdown_impulse = burn_impulse; % return blowdown impulse
% compute total impulse based on blowdown impulse and required prop
 mass
projected_total_impulse=burn_impulse*(bulk_prop_mass/burn_mass);

% compute impulse-weighted specific impulse
weighted_Isp = (dot(isp_vec, thrust_vec))/sum(thrust_vec);

% compute mean thrust
mean_thrust = mean(thrust_vec);

end
```

Published with MATLAB® R2020b

Thrust Calculation

```
function [F] = thrust_calc(mdot,v_e, lambda, P_in, M_e,gamma, D_t,
 rat)
%Calculates engine thrust based on mdot and exit velocity
%source: RPE
A_e=rat*D_t^2 * pi/4;
comp1=(1+((gamma-1)/2)*M_e^2)^(gamma/(gamma-1));
P_e = P_in/comp1;
F= lambda*mdot*v_e + A_e*P_e;


end
```

Published with MATLAB® R2020b

Specific Impulse Calculation

```
function [I_sp] = isp_calc(F,mdot)
%Calculates specific impulse
%source: RPE
g=9.81; %m/s^2
I_sp=F/(mdot*g);


end
```

Published with MATLAB® R2020b

Temperature Update

```
function [T_updated,q_lost] =
 update_T(T,V,n,k,mdot,delta_t,M,T_bulk,k_ins,A_sphere,L,R)
%Updated intermediary tank pressure by one timestep.
%Assumptions: Isentropic flow, ideal gas
%source: https://www.et.byu.edu/~wheeler/Tank_Blowdown_Math.pdf
q_lost = delta_t*k_ins * A_sphere * (T - T_bulk) / L;

mass_lost=mdot*delta_t;
moles_lost=mass_lost/M; %M = molar mass of propellant
old_density=n*M/V;
new_density=(n-moles_lost)*M/V;
Cv=R/(k-1);
T_lost = q_lost/(n*M*Cv);
T_updated=T*(new_density/old_density)^(k-1) - T_lost;
%T_updated=T*(new_density/old_density)^(k-1);


end
```

Published with MATLAB® R2020b

Pressure Update

```
function [P_updated] = update_P(P,V,n,k,mdot,delta_t,M)
%Updated intermediary tank pressure by one timestep.
%Assumptions: Isentropic flow, ideal gas
%source: https://www.et.byu.edu/~wheeler/Tank_Blowdown_Math.pdf
mass_lost=mdot*delta_t;
moles_lost=mass_lost/M; %M = molar mass of propellant
old_density=n*M/V;
new_density=(n-moles_lost)*M/V;

P_updated=P*(new_density/old_density)^k;

end
```

Published with MATLAB® R2020b

Mass Flowrate Calculation

```
function [m_dot] = mdot_calc(P_tank, T_tank, k, D_throat, R_spec, Cd)
%mdot_calc - calculate the instantaneous mass flow rate
% given tank conditions and nozzle geometry


% calculate throat area
A_t = pi * D_throat^2 / 4;

% calculate M_dot from RPE eq. 3-24
m_dot = Cd * A_t * P_tank * k * sqrt( (2 / (k+1))^((k+1) / (k-1)) )...
    / sqrt( k * R_spec * T_tank );

end
```

Published with MATLAB® R2020b

Exit Velocity Calculation

```
function [v_e] = exit_velocity_calc(T_inlet,R,k,M_exit)
%Calculates exit velocity of propellant from nozzle
%source: ASTE 470 notes

T_e=T_inlet/(1+(((k-1)/2)*M_exit^2));
v_e=M_exit*sqrt(k*R*T_e);

end
```

Published with MATLAB® R2020b

Molar Update Calculation

```
function [n_updated] = update_n(n,mdot,delta_t,M)
%Updates number of moles in intermediary propellant tank by one
 timestep
%Assumptions: Isentropic flow, ideal gas
mass_lost=mdot*delta_t;
moles_lost=mass_lost/M; %M = molar mass of propellant
n_updated=n-moles_lost;

end
```

Published with MATLAB® R2020b

Table of Contents


```
function [maxtemp] = maxtemp(V_intermed,t_ins)
```

Key Pointers

```
% Assumptions:
% - Heat energy transfer into R134a is IDEAL, WITH losses i.e. <100%
 of enegry outputted from the
% heater is inputted into the propellant,constant heat output of
 heater (fixed W_input),
% - Energy saturation of each thermal boundar assumed to be
 INSTANTANEOUS for a given timestep
% - Heater contacts <100% of outer tank surface and therefore a given
% proportion of the tank's inner surface area is being heated EVENLY,
 and at the same rate
% - LINEAR increase in both Cv and h_conv for given range of
 temperatures
% - 1-DIMENSIONAL heat conduction between prop, tank walls,
 insulation, and
% environment

% Logic Flow: Tracking isochoric internal energy/enthalpy increase of
 gaseous R134a, based on Q_dot from
% convective/conductive heat transfer equation and size of time
 increment
% Losses included using finite thickness conductive material equation,
% and are removed from total (Q_tot = Q_in - Q_losses for give dt)
```

Input Parameters (TARGET STATES)

n = 0.002 mol State 1: 0.000462 kg of R134a at 5 deg C and 40 psi (determines IC's) State 2: 0.000462 kg of R134a at 650 deg C and 150 psi (determines end state based on target pressure)

```
R_uni = 8.314; % unversal gas constant [J/K-mol]
M = 102.03/1000; %molar mass of propellant [kg/mol]
R = R_uni/M; %propellant-specific gas constant

T_env = 273.15;  % assumed minimum temperature of cubesat environment
 (LEO)
```

Maximum Temperature Calculation (Transient Thermal Analysis)

```
T_prop = 273.15;          %sets initial temperature of propellant @
 State 1

T_heater = 273.15;    %IC for temperature of heater
T_tank = 273.15;    %IC for temperature of the tank
T_ins = 273.15;     %IC for temperature of the insulation (average)


% h_i = 253390*10^3;  %starting enthalpy [J/kg] of R134a at State 1
% h_f = 280630*10^3;  %target enthalpy of R134a at State 2

P = 310264; %starting pressure [Pa] assumed to start at P_tank#1

% m_prop=0.006/2; %initial propellant mass [kg]

V = V_intermed; %internal volume of intermediary tank [m^3]
t_heater = 8.2*10^-6; %heater thickness  [m]
% w_heater = 0.01935;    %heater width (wrapped around tank evenly)
% l_heater = 0.0124;     %heater length
t_tank = 0.000508;  %Al tank thickness
%t_ins = t_ins; %0.00603;       %Aerogel insulation thickness
length_spacer = t_ins;

ID_tank = 2*(V/(4*pi/3))^(1/3); %assuming a SPHERE shaped tank
SA_tank = 4*pi*(ID_tank/2+t_tank)^2;
SA_tank_inner = 4*pi*(ID_tank/2)^2;
SA_sys = (4*pi*(ID_tank/2+t_ins+t_tank)^2);

%SA_tank = %((V^(1/3)+2*t_tank)^2)*6; %assuming a CUBE shaped tank
%SA_tank_inner = ((V^(1/3))^2)*6;
%SA_sys = ((V^(1/3)+2*t_ins+2*t_tank+t_heater)^2)*6;

SA_heater = SA_tank;  %CONTACT SA b/w heater and tank -- assume side
 panels of unit cube holding tank are wrapped with heating foil



% h_conv_i = 0.0119;  %starting convective heat trans. coeff. [W/
m^2*K]of propellant at State 1
% h_conv_f = 0.0574;  %starting convective heat trans. coeff of prop.
 at State 2

Cv_i = 750;      % starting isochoric heat capacity at state 1 [J/
kg*K]
Cv_f = 1300;      % target iso. heat capacity at state 2 (from R134a
 table)
Cv_heater = 461; %heat capacity of nichrome wire
%Cv_tank = 900;   %heat capacity of aluminum
Cv_tank = 490; % heat capacity of 316L SS
Cv_ins = 2000;   %heat capacity of aerogel

k_ins = 0.015;      %thermal conductivity of aerogel [W/m*K]
%k_tank = 205;       %thermal cond. of aluminum tank
k_tank = 23;        % thermal cond. of 316L SS
```

```
k_heater = 11.3;    %thermal cond. of nichrome
k_R134a_1 = 0.011;
k_R134a_2 = 0.0421;
%k_spacer = 2.7;
k_spacer = k_tank;
SA_ins = SA_tank;   %conductive boundary between aluminum tank and
 insulation

rho_heater = 8400;     %density of nichrome [kg/m^3]
rho_ins = 20;          %density of aerogel
%rho_tank = 2700;       %density of aluminum tank
rho_tank = 8000;        % density of 316L SS tank
rho_spacer = 5680;
m_ins = (4*pi/3)*((ID_tank/2+t_tank+t_ins)^3-
(ID_tank/2+t_tank)^3)*rho_ins;
m_tank = (4*pi/3)*((ID_tank/2+t_tank)^3-(ID_tank/2)^3)*rho_tank;
n = (P*V)/(T_prop*R_uni);    %determines # moles of propellant present
 in Tank #2 at State 1
m_prop = n*M;                %computes mass of propellant from n moles
V_heater = (4/3)*pi*((ID_tank/2+t_tank+t_heater)^3-
(ID_tank/2+t_tank)^3);
m_heater = rho_heater*V_heater;

V_forcon = (pi*0.001^2)*(t_ins+t_tank)-(pi*0.0005^2)*(t_ins+t_tank);
V_aftcon = (pi*0.001^2)*(t_ins+t_tank)-(pi*0.0005^2)*(t_ins
+t_tank)+(pi*0.002^2)*(0.0005)-(pi*0.005^2)*(0.0005);
m_forcon = V_forcon*rho_tank;
m_aftcon = V_aftcon*rho_tank;
m_vaporizer = 0.00006;
V_spacer = length_spacer*(pi*0.0015875^2-pi*0.0005^2);
m_spacer = rho_spacer*V_spacer;

dt = 0.1;
t_final = 519; %in seconds
```

Compute initial temperature, thermal properties, and heat flux for iterations

```
Q_dot_IN = 5;   %power output of heaetr [Watts // J/s]
Q_IN = Q_dot_IN*dt;
Q_OUT = 0;      %initial losses, zero since (T_tank-T_env) = 0
Cv_prop = Cv_i;
% h_conv_prop = h_conv_i;
T_sys = 273.15;          %for method 3
```

Initialize Loop Variables and Storage Vectors

```
i=1;

Q_dot_OUT_ins = 0;
Cv_vec = zeros(1,t_final/dt);
```

```
Q_dot_OUT_vec = zeros(1,t_final/dt);
T_prop_vec = zeros(1,t_final/dt);
T_heater_vec = zeros(1,t_final/dt);
T_tank_vec = zeros(1,t_final/dt);
T_ins_vec = zeros(1,t_final/dt);
Q_in_prop_vec = zeros(1,t_final/dt);
Q_in_heater_vec = zeros(1,t_final/dt);
Q_OUT_ins_vec = zeros(1,t_final/dt);
Q_in_tank_vec = zeros(1,t_final/dt);
Q_net_vec = zeros(1,t_final/dt);
T_sys_vec = zeros(1,t_final/dt);
Q_in_NET_vec = zeros(1,t_final/dt);
Q_OUT_spacer_vec = zeros(1,t_final/dt);

time_vec = linspace(0,t_final,t_final/dt+1);
```

METHOD 3 -- Heater, tank, and propellant layers LUMPED (Cv's combined, losses still included)

```
m_total = m_tank+m_heater+m_prop; %+m_forcon+m_aftcon+m_vaporizer

for t = 0:dt:t_final

Cv_lumped = ((m_tank)/m_total)*Cv_tank + (m_prop/m_total)*Cv_prop +
 (m_heater/m_total)*Cv_heater; %m_aftcon+m_forcon+m_vaporizer+

Q_in_NET = Q_IN-Q_OUT;
Q_in_sys = Q_in_NET;

delta_T_sys = Q_in_sys/(m_total*Cv_lumped);
T_sys = T_sys + delta_T_sys;

% assume spacer = McMaster 5560K46 (.05"OD, .042" ID)
Q_dot_OUT_spacer = 2*k_spacer*(pi*0.000635^2-pi*0.000533^2)*(T_sys-
T_env)/(length_spacer);
Q_dot_OUT_ins = (4*pi*k_ins*(ID_tank/2+t_tank)*(ID_tank/2+t_tank
+t_ins)*(T_sys-T_env))/(t_ins);  %1D transfer through thin walled
 spherical shell
%Q_dot_OUT = (k_ins*SA_sys*(T_sys-T_env))/(t_ins);  %1D transfer
 through finite plane (SA's equated)
Q_OUT = Q_dot_OUT_ins*dt+Q_dot_OUT_spacer*dt;

Cv_prop = Cv_prop + (Cv_f-Cv_i)/(t_final/dt);

T_sys_vec(i) = T_sys;
Q_in_NET_vec(i) = Q_in_NET;
Q_OUT_ins_vec(i) = Q_dot_OUT_ins*dt;
Q_OUT_spacer_vec(i) = Q_dot_OUT_spacer*dt;

i=i+1;
```

```
end

A = sum(Q_OUT_ins_vec);
P2 = (n*R*T_sys)/V;
% ASSUME lumped thermal mass

%ignore thermal diffusivity, assume signular thermal mass where all
%components heat evenly, and find general heating cuve for tank,
 heater,
%and propellant!
```

Plotting

```
%{
figure
plot(time_vec,T_sys_vec-273.15);
xlabel('Time [sec]', 'Interpreter', 'latex')
ylabel('Temperature [C]', 'Interpreter', 'latex')
xlim([0 t_final])

% figure
% plot(time_vec,Q_in_NET_vec);
% title("Energy Transfer Rate IN vs Time")
% xlabel('Time  [seconds]'),ylabel('Q_in  [Joules]')
% legend('Q_i_n_-_N_E_T')
% xlim([0 t_final])

figure
plot(time_vec,Q_OUT_ins_vec);
hold on
plot(time_vec,Q_OUT_spacer_vec);
xlabel('Time [sec]'),ylabel('Thermal Energy Loss [J]', 'Interpreter',
 'latex')
legend('$Q_{out, ins}$','$Q_{out, con}$', 'Interpreter', 'latex')
xlim([0 t_final])


% figure
% plot(time_vec,Q_in_heater_vec);
% hold on
% plot(time_vec,Q_in_prop_vec);
% hold on
% plot(time_vec,Q_OUT_vec);
% hold on
% plot(time_vec,Q_in_tank_vec,'--','color','k');
% title("Energy Transfer Rate vs Time")
% xlabel('Time  [seconds]'),ylabel('Q_in  [Joules]')
% legend('Q_I_N_-_h_e_a_t','Q_I_N_-_p_r_o_p','Q_O_U_T','Q_I_N_-
_t_a_n_k')
% xlim([0 t_final])
```

```
%% EXTRANEOUS

% h_conv_vec = zeros(1,t_final/dt);
% delta_T_prop_vec = zeros(1,t_final/dt);
% delta_T_heater_vec = zeros(1,t_final/dt);
% delta_T_tank_vec = zeros(1,t_final/dt);


% Q_dot_prop_vec = zeros(1,t_final/dt);
% Q_in_prop_vec = zeros(1,t_final/dt);
% Q_dot_heater_vec = zeros(1,t_final/dt);
% Q_in_heater_vec = zeros(1,t_final/dt);
% Q_dot_tank_vec = zeros(1,t_final/dt);
% Q_in_tank_vec = zeros(1,t_final/dt);
% Q_out_ins_vec = zeros(1,t_final/dt);


% Q_dot_prop = h_conv_prop*SA_tank*(T_tank-T_prop);
% Q_in_prop = Q_dot_prop*dt;
% delta_T_prop = Q_in_prop/(Cv_prop*m_prop);  %temperature change of
 propellant for given Q_in added to system
% Q_dot2 = h_conv*SA_heat2*(T_wall-T_prop2);
% Q_in2 = Q_dot2*delta_t;
% delta_T2 = Q_in2/(Cv*m_prop)

%     T_heater = T_heater + delta_T_heater_i;
%
%     Q_dot_tank = (k_tank*SA_tank*(T_heater-T_tank))/t_tank;
%     Q_in_tank = Q_dot_tank*dt;
%     delta_T_tank = Q_in_tank/(m_tank*Cv_tank);
%     T_tank = delta_T_tank + T_tank;
%
%     Q_dot_prop = h_conv_prop*SA_tank*(T_tank-T_prop);
%     Q_in_prop = Q_dot_prop*dt;
%     delta_T_prop = Q_in_prop/(Cv_prop*m_prop);
%     T_prop = T_prop+delta_T_prop;
%     delta_T_prop_vec(i) = delta_T_prop;
%     T_prop_vec(i) = T_prop;
%     Q_dot_prop_vec(i) = Q_dot_prop;
%     Q_in_prop_vec(i) = Q_in_prop;
%
%
%
%     Q_in_final_tank = (Q_in_tank-Q_in_prop);
%     delta_T_final_tank = Q_in_final_tank/(Cv_tank*m_tank);
%     T_tank = T_tank-Q_in_tank/(m_tank*Cv_tank)+delta_T_final_tank;
%     T_tank_vec(i) = T_tank;
%     Q_in_tank_vec(i) = Q_in_final_tank;
% %     Q_dot_tank_vec(i) = Q_dot_tank;
%
%
```

```
%     Q_dot_ins1 = (k_ins*SA_heater*(T_heater-T_env))/(t_ins);
%     Q_dot_ins2 = (k_ins*(SA_tank-SA_heater)*(T_tank-T_env))/(t_ins);
%     Q_dot_ins = Q_dot_ins1+Q_dot_ins2;
%     Q_out_ins = Q_dot_ins*dt;
%     Q_out_ins_vec(i) = Q_out_ins;
%
%     Q_in_final_heater = Q_dot_heater_i*dt-Q_in_final_tank-Q_in_prop-
Q_out_ins;
%     delta_T_heater = Q_in_final_heater/(Cv_heater*m_heater);
%     T_heater = T_heater-delta_T_heater_i+delta_T_heater;
%     T_heater_vec(i) = T_heater;
%
%     h_conv_vec(i) = h_conv_prop;
%     h_conv_prop = h_conv_prop + (h_conv_f-h_conv_i)/(t_final/dt);
%
%     Cv_vec(i) = Cv_prop;
%     Cv_prop = Cv_prop + (Cv_f-Cv_i)/(t_final/dt);
%
%
%
% %     Q_in_vec2(i) = Q_in2;
% %     Q_in2 = Q_dot2*delta_t;
%
% %      delta_T_vec2(i) = delta_T2;
% %     delta_T2 = Q_in2/(Cv*m_prop);
%
% %       T_prop_vec2(i) = T_prop2;
% %     T_prop2 = T_prop2+delta_T2;
%
% %     Q_dot_vec2(i) = Q_dot2;
% %     Q_dot2 = h_conv*SA_heat2*(T_wall2-T_prop2);
%
%     i=i+1;
% end

% P_final = n*R_uni*T_prop/V
% Q_in_TOT = sum(Q_in_prop_vec)

% P_final2 = n*R_uni*T_prop2/V
% Q_in_TOT2 = sum(Q_in_vec2)
%}
maxtemp=T_sys_vec(length(T_sys_vec));

end
```

Published with MATLAB® R2020b

Optimization Code

```
%%%%%%%%%%%%%%%%%%%%   Prepare environment   %%%%%%%%%%%%%%%%%%%%
clc; clear variables; close all;

% Define variables
num=20; % number of datapoints along each sweep direction
Dt = 0.0004; % nozzle throat diameter [m]
V_range = linspace(0.000003, 0.000006, num);%intermediate tank volume
 [m^3]
                                                % upper lim set by CAD
L_range = linspace(0.001, 0.04, num); %allowable volume for the
 combined
%intermediate vessel and insulation

impulse=zeros(num,num); %initialize impulse array
R_universal=8.314; % J/(mol-K)

blowdown = impulse; %initialize blowdown impulse array
P_0 = impulse; %initialize pressure array
percent_left = impulse; %initialize percent_left (moles of propellant
 in
%intermediate vessel) array

Bulk_T= 273.15;% K Bulk propellant storage temperature
Bulk_P=310000; %Pa Bulk propellant storage pressure

prop_MM=102.13/1000; %kg/mol Propellant molar mass


T_target = 923.15; % K Desired max temp of insulation
tolerance = 923; %K   Tolerance of solutions (temperature of
 insulation)


lambda=0.989;
%%%%%%%   compute exit Mach number from nozzle area ratio  %%%%%%%
syms M;
g = 1.2; rat = 20;
eqn = (1/M) * ( (2/(g+1) * (1 + ((g-1)/2)*M^2)) )^((g+1)/(2*g-2)) ==
 rat;
M_exit = double( vpasolve(eqn, M, 1.1) );


%%%%%%%%%%%%%%%%%%%%  Main loop  %%%%%%%%%%%%%%%%%%%%

count=1;
max_total_impulse_index = 1; %index of maximum total impulse solution

for i=1:length(L_range)
    disp(i);
    for j=1:length(V_range)

        % compute allowable insulation thickness
```

Optimization Code

```
            r_tank = (3*V_range(j)/(4*pi))^(1/3);
            %L = (3*V_allowable(i)/(4*pi))^(1/3) - r_tank;
            V_allowable = 4*(r_tank+L_range(i))^3*pi/3;

            % compute initial prop mass in the tank
            n=Bulk_P*V_range(j)/(R_universal*Bulk_T);
            m_prop=n*prop_MM;

            % compute max attainable temp at 520 seconds
            T = maxtemp(V_range(j), L_range(i));

            %call nozzle_perf
            [impulse(i,j), blowdown(i,j), P_0(i,j), percent_left(i,j), ...
                weighted_Isp, mean_thrust] = nozzle_perf(T, m_prop, Dt,...
                V_range(j), L_range(i),M_exit, V_allowable,rat,lambda);

         %If the insulation temperature is close enough (from below) to the
         %temperature constraints, and the blowdown impulse is at least 40 mN-
        sec,
         %keep solution
            if (T_target - T < tolerance) && (T_target - T >= 0) && ...
                    blowdown(i,j) >= 0.04

                %store solution parameters
                sol_T(count) = T;
                sol_V_allowable(count) = V_allowable;
                sol_V_tank(count) = V_range(j);
                sol_blowdown(count) = blowdown(i,j);
                sol_total(count) = impulse(i,j);
                sol_mass(count) = m_prop;
                sol_L(count) = L_range(i);
                sol_weighted_Isp(count) = weighted_Isp;
                sol_mean_thrust(count) = mean_thrust;

                if (impulse(i,j) > sol_total(max_total_impulse_index))
                    max_total_impulse_index = count; %store index of
                    %solution with highest total delivered impulse
                end

                count = count + 1;
            end
        end
    end

    format shortE;
    fprintf('Optimum intermediate tank volume: %.4e m^3\n', ...
        sol_V_tank(max_total_impulse_index));
    fprintf(['Optimum volume for combined intermediate tank + ',...
        'insulation: %.4e m^3 \n'], ...
        sol_V_allowable(max_total_impulse_index));
    fprintf('Optimum insulation thickness: %.4e m\n', ...
        sol_L(max_total_impulse_index));
    fprintf('Optimum intermediate tank temperature at 520 sec: %.1f K
    \n', ...
```

Optimization Code

```
    sol_T(max_total_impulse_index));
fprintf('Optimum blowdown impulse: %.1f mN-sec\n', ...
    sol_blowdown(max_total_impulse_index) * 1000);
fprintf('Optimum total impulse: %.1f N-sec\n', ...
    sol_total(max_total_impulse_index));
fprintf('Optimum weighted specific impulse: %.1f sec\n', ...
    sol_weighted_Isp(max_total_impulse_index));
fprintf('Optimum mean thrust: %.1f mN\n', ...
    sol_mean_thrust(max_total_impulse_index)*1000);
fprintf('Initial intermediate tank propellant load: %.4e kg\n', ...
    sol_mass(max_total_impulse_index));
fprintf('Exit Mach number: %.4f \n', ...
    M_exit);

figure
surf(V_range, L_range, impulse, blowdown);
ylabel("Insulation Thickness [m]", 'Interpreter', 'latex');
xlabel("Intermediate Tank Volume [$m^3$]", 'Interpreter', 'latex');
zlabel("Total Impulse [N-s]", 'Interpreter', 'latex');
hcb=colorbar;
hcb.Title.String = "Blowdown Impulse [N-s]";
hcb.Title.Interpreter = 'latex';
%{

figure
scatter(sol_V_tank, sol_total, 20, sol_blowdown, 'filled');
xlabel("Intermediate Tank Volume [$m^3$]", 'Interpreter', 'latex');
ylabel("Total Impulse [N-s]", 'Interpreter', 'latex');
hcb=colorbar;
hcb.Title.String = "Blowdown Impulse [N-s]";
hcb.Title.Interpreter = 'latex';

%}
```

Published with MATLAB® R2020b

Master Equipment List

Master Equipment List | Structure | Fluid

Component	Part Name	Make	Diameter	Length	Quantity	Price Per	Price	Notes
Test Plate	Multipurpose 6061 Aluminum	McMaster		12" x 12"	1	$118.60	$118.60	1-1/4" Thick, 12" x 12"
Bulk Tank	Refillable Propane Tank	Rei	3.75"	8.75"	1	$15.00	$15.00	0.5 Liters
Bulk Tank Holder	Custom 3D Print			5" x 5" x 4"	1	$60.00	$60.00	Filement and Time on Printer
Cradle	Custom 3D Print				1	$50.00	$50.00	Filement and Time on Printer
Intermediate Tank	316 Stainless Steel Shim Stock	McMaster	0.020"	8" x 12"	1	$20.19	$20.19	
Insulation	THERMABLOK AEROGEL INSULATION BLANKET	Thermablock		12" x 12"	1	$300.00	$300.00	Estimate becuase quote needed
Nozzle Block	Multipurpose 6061 Aluminum	McMaster		3/4" Thick x 5" Wide X 6" Long	1	$20.60	$20.60	
Heater	NI050235	Goodfelllow	0.10mm	50mm x 50mm	1	$185.00	$185.00	Nickel Chromium
Propane to NPT	Propane addapter fitting	Home Depot	1/4 "		1	$8.79	$8.79	1" propane to 1/4" NPT
SS 316 Tubing	Smooth-Bore Seamless 316 Stainless Steel Tubing	McMaster	1/8" OD, 0.035" Wall Thickness	3 ft	1	$33.31	$33.31	ID = 1.4mm, OD = 3.175mm
Reducing Elbow	90 Degree Elbow Reducer for 1/4" x 1/8" Tube OD	McMaster	1/4" to 1/8"		1	$47.82	$47.82	Yor-Lok
Elbow	90 Degree Elbow Connector for 1/8" Tube OD	McMaster	1/8"		2	$24.36	$48.72	Yor-Lok
Valve	Hannifin 009-0270-900 Multimedia Valve	Cole-Parmer	1/8"		2	$472.00	$944.00	2-Way NC, 1/8" A-Lok, 24 VDC, 250 psi max
TC	CAIN-18U-6	Omega	1/8"		2	$37.75	$75.50	
TC	CAIN-116U-6	Omega	1/16"		1	$38.81	$38.81	
PT	PX191-150GV5	Omega	1/8"		1	$120.00	$120.00	0-150 PSI
PT	PX191-075GV5	Omega	1/8"		1	$120.00	$120.00	0-75 PSI
						Total	$2,206.34	

Benchtop System Manufacturing Drawings

It is noted that additively manufactured parts do not have manufacturing drawings, as their STP files are sent directly to the printers and no post-machining is assumed.

REVISIONS				
ZONE	REV	DESCRIPTIONS	DATE	APPR
	A	INITIAL RELEASE	XX/XX/XXXX	XXX

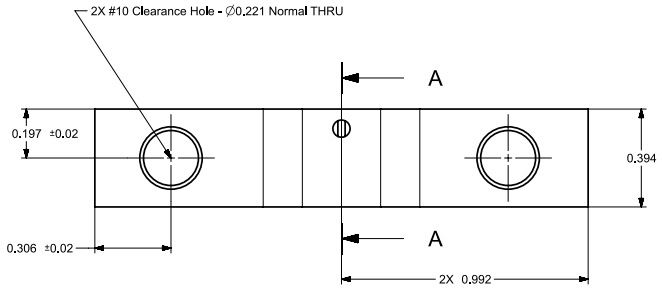

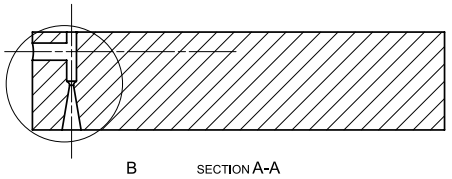

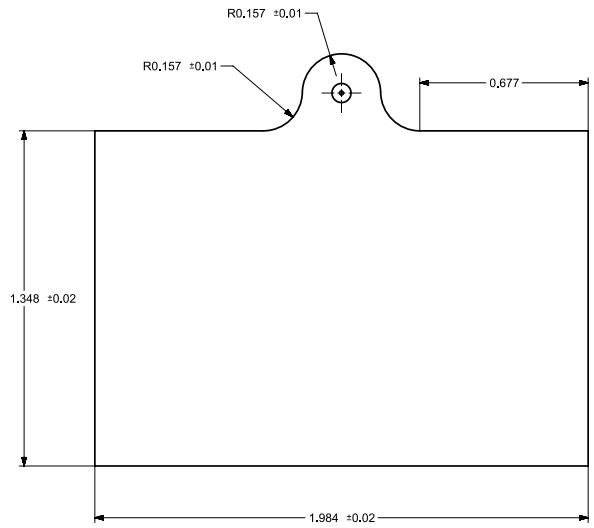

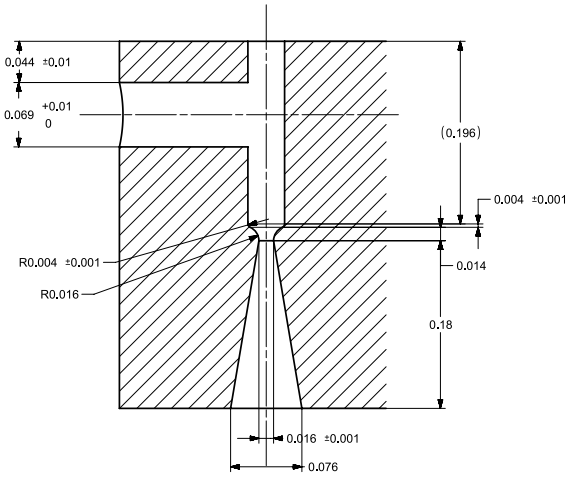

DETAIL B
SCALE 15:1

ITEM	MATERIAL SPEC / VENDOR	DESCRIPTION	PART NUMBER	QTY/ASSY
1				

- PARTS LIST -

UNLESS OTHERWISE SPECIFIED DIMENSIONS ARE IN INCHES
TOLERANCES ARE:
DECIMALS: .X = ±0.1, .XX = ±0.03, .XXX = ±0.005
ANGLES: ALL = ±0.5°
UNDIMENSIONED FEATURES ±0.03 DO NOT SCALE PRINT
REMOVE BURRS AND SHARP EDGES
CBORE AND SPOTFACE EQUIVALENT TO CORNER RADIUS.
R = 0.031 FOR DIA THRU 1.25
R = 0.062 FOR DIA > 1.25
R = 0.031 MIN FOR MATCH PARTS
MACHINED ROUGHNESS = 0.125 RMS MAX

	NAME	DATE
DRAWN BY	S. POWERS	11/17/20
DESIGN BY	C. POWERS	
DESIGN CHECK		
MFG CHECK BY		
APPROVED BY		

THIRD ANGLE PROJECTION
INTERPRET DRAWING IN ASSOCIATION WITH ASME Y14.5-2018

AME 441

GROUP # 9

TITLE: NOZZLE

SIZE: D | DWG NO.: Benchtop Nozzle | SHEET REV: A

SCALE 1:1 | SHEET 1 OF 1

REVISIONS				
ZONE	REV	DESCRIPTIONS	DATE	APPR
	A	INITIAL RELEASE	XX/XX/XXXX	XXX

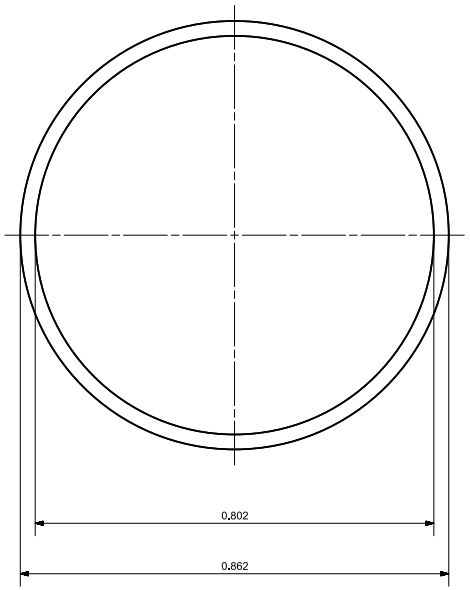

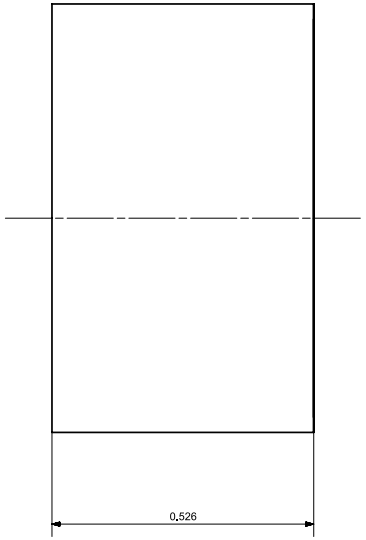

1				
PART NUMBER	DESCRIPTION		MATERIAL SPEC / VENDOR	ITEM
QTY/ASSY	- PARTS LIST -			

UNLESS OTHERWISE SPECIFIED DIMENSIONS ARE IN INCHES
TOLERANCES ARE:
DECIMALS:
.X = ±0.1
.XX = ±0.03
.XXX = ±0.005
ANGLES:
ALL = ±0.5°
UNDIMENSIONED FEATURES ±0.03
DO NOT SCALE PRINT
REMOVE BURRS AND SHARP EDGES
CBORE AND SPOTFACE
EQUIVALENT TO CORNER RADIUS.
R = 0.031 FOR DIA THRU 1.25
R = 0.062 FOR DIA > 1.25
R = 0.031 MIN FOR MATCH PARTS
MACHINED ROUGHNESS = 0.125 RMS MAX

	NAME	DATE
DRAWN BY	S. POWERS	11/17/20
DESIGN BY	M. MASTRANGELO	
DESIGN CHECK		
MFG CHECK BY		
APPROVED BY		

THIRD ANGLE PROJECTION
INTERPRET DRAWING IN ASSOCIATION WITH ASME Y14.5-2018

AME 441

GROUP # 9

TITLE: INTERM. TANK BARREL

SIZE	DWG NO.	SHEET REV
D	intermed_vessel_barrel	A
SCALE 1:1		SHEET 1 OF 1

REVISIONS				
ZONE	REV	DESCRIPTIONS	DATE	APPR
	A	INITIAL RELEASE	XX/XX/XXXX	XXX

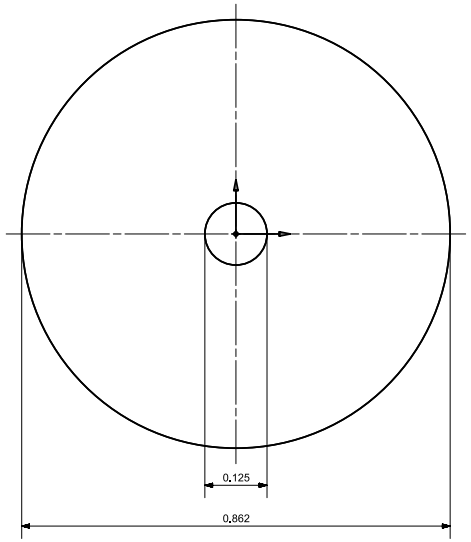

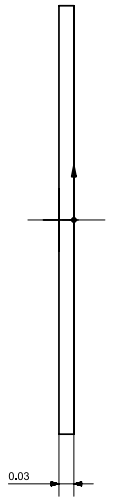

QTY/ASSY	PART NUMBER	DESCRIPTION	MATERIAL SPEC / VENDOR	ITEM
		- PARTS LIST -		

UNLESS OTHERWISE SPECIFIED DIMENSIONS ARE IN INCHES
TOLERANCES ARE:

DECIMALS:
.X = ±0.1
.XX = ±0.03
.XXX = ±0.005

ANGLES:
ALL = ±0.5°

UNDIMENSIONED FEATURES ±0.03
DO NOT SCALE PRINT

REMOVE BURRS AND SHARP EDGES
CBORE AND SPOTFACE
EQUIVALENT TO CORNER RADIUS.

R = 0.031 FOR DIA THRU 1.25
R = 0.062 FOR DIA > 1.25
R = 0.031 MIN FOR MATCH PARTS

MACHINED ROUGHNESS = 0.125 RMS MAX

	NAME	DATE
DRAWN BY	S. POWERS	11/17/20
DESIGN BY	C. POWERS	
DESIGN CHECK		
MFG CHECK BY		
APPROVED BY		

THIRD ANGLE PROJECTION

INTERPRET DRAWING IN ASSOCIATION WITH ASME Y14.5-2018

AME 441

GROUP # 9

TITLE: INTERM. VESSEL CAP

SIZE	DWG NO.	SHEET REV
D	intermed_cap	A

SCALE 1:1 | SHEET 1 OF 1

Gantt Chart

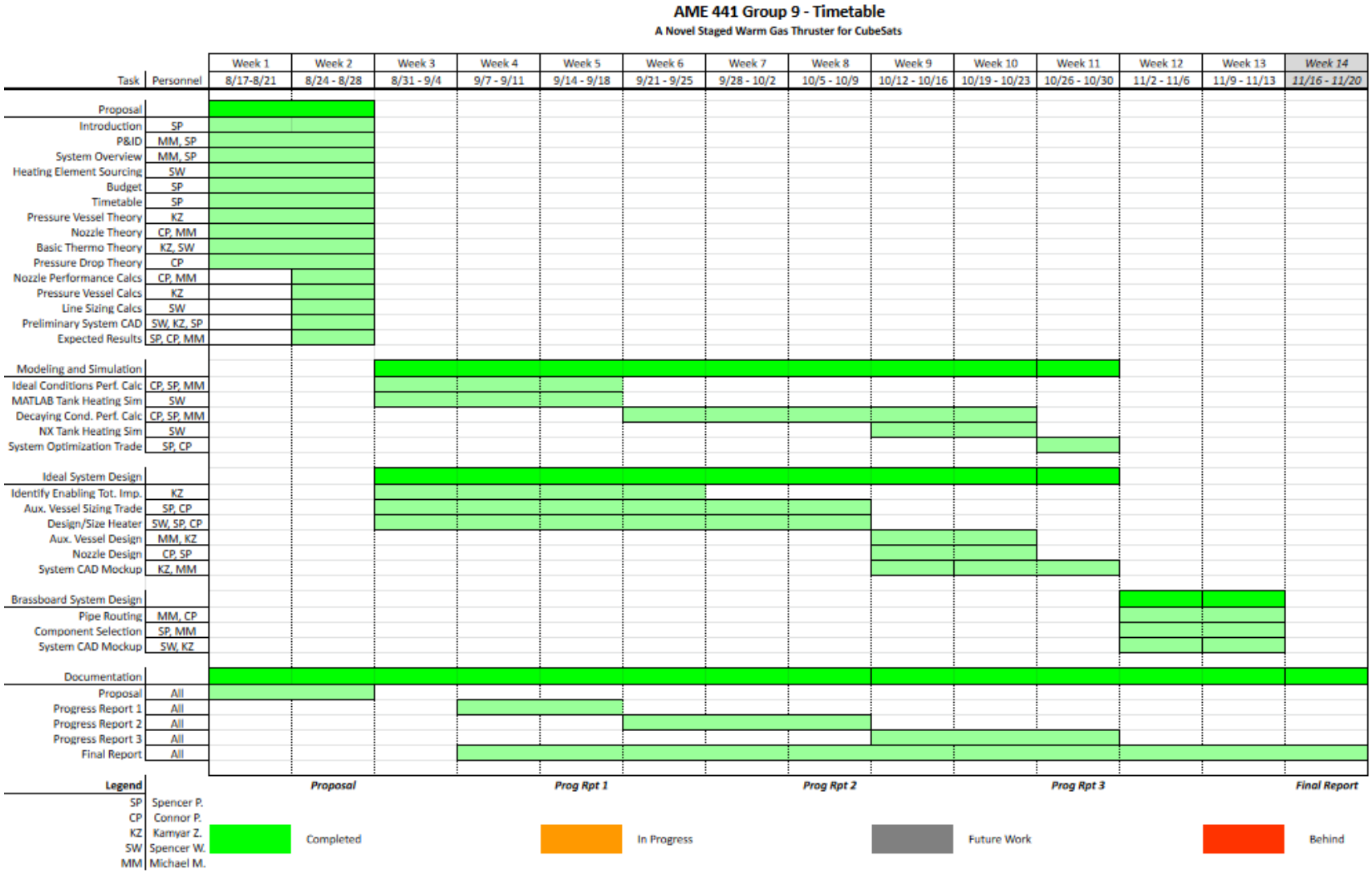
AME 441 Group 9 - Timetable
A Novel Staged Warm Gas Thruster for CubeSats
Task
Personnel
Week 1 8/17-8/21
Week 2 8/24 - 8/28
Week 3 8/31 - 9/4
Week 4 9/7 - 9/11
Week 5 9/14 - 9/18
Week 6 9/21 - 9/25
Week 7 9/28 - 10/2
Week 8 10/5 - 10/9
Week 9 10/12 - 10/16
Week 10 10/19 - 10/23
Week 11 10/26 - 10/30
Week 12 11/2 - 11/6
Week 13 11/9 - 11/13
Week 14 11/16 - 11/20
Proposal
Introduction SP
P&ID MM, SP
System Overview MM, SP
Heating Element Sourcing SW
Budget SP
Timetable SP
Pressure Vessel Theory KZ
Nozzle Theory CP, MM
Basic Thermo Theory KZ, SW
Pressure Drop Theory CP
Nozzle Performance Calcs CP, MM
Pressure Vessel Calcs KZ
Line Sizing Calcs SW
Preliminary System CAD SW, KZ, SP
Expected Results SP, CP, MM
Modeling and Simulation
Ideal Conditions Perf. Calc CP, SP, MM
MATLAB Tank Heating Sim SW
Decaying Cond. Perf. Calc CP, SP, MM
NX Tank Heating Sim SW
System Optimization Trade SP, CP
Ideal System Design
Identify Enabling Tot. Imp. KZ
Aux. Vessel Sizing Trade SP, CP
Design/Size Heater SW, SP, CP
Aux. Vessel Design MM, KZ
Nozzle Design CP, SP
System CAD Mockup KZ, MM
Brassboard System Design
Pipe Routing MM, CP
Component Selection SP, MM
System CAD Mockup SW, KZ
Documentation
Proposal All
Progress Report 1 All
Progress Report 2 All
Progress Report 3 All
Final Report All
Proposal
Prog Rpt 1
Prog Rpt 2
Prog Rpt 3
Final Report
Legend
SP Spencer P.
CP Connor P.
KZ Kamyar Z.
SW Spencer W.
MM Michael M.
Completed
In Progress
Future Work
Behind